GSI-94-44
PREPRINT
AUGUST 1994

FERMIONIC MOLECULAR DYNAMICS FOR GROUND STATES AND COLLISIONS OF NUCLEI

H. FELDMEIER, K. BIELER, J. SCHNACK

(Submitted to Nuclear Physics A)

Gesellschaft für Schwerionenforschung mbH
Postfach 110552 · D-64220 Darmstadt · Germany

Fermionic Molecular Dynamics for ground states and collisions of nuclei

H. Feldmeier, K. Bieler and J. Schnack

Gesellschaft für Schwerionenforschung mbH, Postfach 110 552, D-64220 Darmstadt

Contents

Article published in Elsevier Science 0 (1994) 1–0

Fermionic Molecular Dynamics for ground states and collisions of nuclei

H. Feldmeier, K. Bieler and J. Schnack

Gesellschaft für Schwerionenforschung mbH, Postfach 110 552, D-64220 Darmstadt

Abstract

The antisymmetric many-body trial state which describes a system of interacting fermions is parametrized in terms of localized wave packets. The equations of motion are derived from the time-dependent quantum variational principle. The resulting Fermionic Molecular Dynamics (FMD) equations include a wide range of semi-quantal to classical physics extending from deformed Hartree–Fock theory to Newtonian molecular dynamics. Conservation laws are discussed in connection with the choice of the trial state. The model is applied to heavy-ion collisions with which its basic features are illustrated. The results show a great variety of phenomena including deeply inelastic collisions, fusion, incomplete fusion, fragmentation, neck emission, promptly emitted nucleons and evaporation.

1 Introduction and summary

The mean-field picture has been applied successfully to low energy heavy-ion collisions where the velocity of the nucleons is large compared to the surface velocity of the mean field. For beam energies $E_{LAB} - E_{CB} \gtrsim 50$ AMeV above the Coulomb barrier the relative velocity between the two nuclei exceeds the Fermi velocity of the nucleons inside the nuclei. Thus for $E_{LAB} - E_{CB} \gtrsim 15$ AMeV, which corresponds to about half the Fermi velocity, one expects that the nucleons are too slow to establish a common mean field. This is reflected by the observation of large fluctuations in the final mass distribution or in other observables. Therefore a molecular dynamics model, which is not based on the mean-field assumption, seems to be most promising for a dynamical description of these collisions.

Long before the observation of multifragmentation reactions one has attempted to set up classical molecular dynamics models to describe the collision of nuclei [1–3]. While collective degrees of freedom like the center of mass of a

Article published in Elsevier Science 0 (1994) 1–0

nucleus can be treated classically, the trajectories of the individual nucleons cannot. This is readily seen from the two conditions for a classical treatment which are:

a) The de Broglie wavelength in the relative motion of two nucleons should be shorter than the variations in the two-body interaction.

Considering the range of the nucleon-nucleon potential, 0.3 fm may serve as an upper limit for the de Broglie wavelength

$$\lambda_{Broglie} = \frac{2\pi}{k} \leq 0.3 \text{ fm} \rightarrow k \geq 20 \text{ fm}^{-1}.$$

This localization implies that the relative momenta k of the nucleons should be greater than 4000 MeV/c which is never fulfilled for nucleons in the same nucleus as the Fermi momentum is only 300 MeV/c. The necessary relative momenta are reached in collisons with $E_{LAB} > 8$ AGeV but only for nucleons which are in the target and in the projectile, respectively.

b) The wave packet should not spread too much during the reaction time.

As an estimate one may take the time in which a freely moving packet of minimal uncertainty has doubled its spatial width. In the rest frame of the particle with mass m_N= 939 MeV/c^2 this time is given by

$$\tau_{reaction} < 2m_N\sigma_0^2 \approx 1\text{fm/c}$$

which implies for an initial width of $\sigma_0 = 0.3$ fm a time scale of 1 fm/c. Again this condition is only met for relativistic collisions.

Therefore one must conclude that a naive non-quantal molecular dynamics picture where the nucleons are represented by points in the phase space cannot be applied to non-relativistic heavy-ion collisions below about 8 AGeV beam energy.

Quantum Molecular Dynamics (QMD) [5,6] attributes instead of a point to each nucleon a gaussian phase-space distribution with a time-independent width but still uses classical equations of motion for their mean positions $\boldsymbol{r}_k$ and mean momenta $\boldsymbol{p}_k$. These equations of motion contain a mean-field force and a fluctuating force generated with random numbers. While in the fluctuating force (collision term) the Pauli exclusion principle for identical fermions is taken notice of by means of a "Pauli blocker", the mean-field force is that of distinguishable particles.

Antisymmetrized Molecular Dynamics (AMD) [7,8] is based on the same concept as QMD but the smooth part in the motion of the nucleons is described by the fermionic equations of motion [10] but using fixed widths. Also the

"Pauli blocker" in the collision term is improved as it refers to approximate canonical variables rather than to the parameters $\boldsymbol{r}_k$ and $\boldsymbol{p}_k$.

Fermionic Molecular Dynamics (FMD), introduced in ref. [10], takes the following view: The closest quantum analogue to a point in the single-particle phase space representing a classical particle is a wave packet well localized in phase space. The analogue to a point in the many-body phase space representing several classical particles is a many-body state which is the product of localized single-particle packets. If the particles are identical fermions, the analogue is the projection of this many-body state onto the subspace antisymmetric with respect to particle exchange. For identical bosons it is the projection onto the symmetric subspace. The wave packets are given by a set of parameters including mean position $\boldsymbol{r}_k$, mean momentum $\boldsymbol{p}_k$, complex width a_k and spin direction $\boldsymbol{\sigma}_k$. Furthermore, the equations of motion for these parameters are derived from a quantum variational principle.

Using wave packets automatically guarantees that the Heisenberg uncertainty principle is not violated by the model. Using antisymmetrized many-body trial states automatically guarantees that the Pauli exclusion principle is respected by the model. However, the ansatz of antisymmetrized wave packets does not exclude the classical molecular dynamics picture. Actually the fermionic equations of motion given in section 2.5 go smoothly over into Newton's classical equations of motion when conditions a) and b) for classical motion are fulfilled.

Since in FMD the energy is the expectation value of a Hamilton operator calculated with an antisymmetric many-body trial state, the ground state is in a natural way the state which has minimal energy with respect to variations in the parameters. Hence it is stationary and all parameters are time-independent. The momentum distributions of ground states displayed in section 3.1 show that – besides the important effects of antisymmetrization – the Fermi motion is essentially due to the width of the wave packets and not due to non-zero mean momenta. Section 3.2 illustrates how antisymmetrization also introduces shell effects and delocalization of the fermions. These quantum effects are certainly not in classical molecular dynamics models and are also not in models which include effects of the Pauli principle only by blocking occupied states in the collision term (QMD).

The FMD ground states have to be treated like intrinsically deformed Hartree-Fock states. Section 3.5 defines an ensemble by adding coherently individual events which differ in their initial orientations of the ground states. It is shown that the final states can be averaged incoherently because they become orthogonal due to the semi-quantal time evolution.

To simulate the effect of the antisymmetrization on the classical trajectories many authors [2,11–14] add to the hamiltonian a two-body "Pauli potential"

which is supposed to keep the fermions apart from each other in phase space. Studying in section 3.3 the effect of antisymmetrization on the trajectories renders doubts in this approximate treatment of fermionic dynamics. From the FMD equations it is possible to define locally canonical pairs of variables. Expressing the hamiltonian in terms of these canonical variables defines the proper "Pauli hamiltonian" which is not the classical hamiltonian plus a "Pauli potential". A canonical variable depends in general on all the variables of all wave packets which makes it impossible to regard it as a coordinate of a single nucleon. Only when the wave packets have no overlap classical and fermionic canonical coordinates coincide.

Numerical solutions of the FMD equations show a rich variety of phenomena, the most prominent being the observation of large fluctuations in the final stage for collisions with identical impact parameter and beam energy but different initial orientations of the nuclei. On short time scales (100 fm/c) there are promptly emitted particles, multifragmentation and incomplete fusion while sequential decay and evaporation of nucleons from the excited fragments occur on longer time scales (calculations have been done up to 2000 fm/c). Emission of nucleons and intermediate mass fragments from the neck region are observed. Not all these phenomena are shown in sections 3.4 and 3.6. Instead of displaying a few snap shots at different times of the one-body density a much better understanding of the collisions can achieved by looking at the time evolution in terms of a computer animation which displays the shape and positon of each wave packet as a function of time. A diskette can be ordered from the authors which runs on an IBM compatible personal computer and contains more reactions than could be included in this paper.

2 The Fermionic Molecular Dynamics Model

The Fermionic Molecular Dynamics (FMD) model is built on three components. The first is an antisymmetrized many-body trial state which contains the essential degrees of freedom in the many fermion system. These are represented by a manifold of parameters which specify the trial state uniquely. The simplest case is a single Slater determinant but one could as well think of a correlated many-body state which takes care of the repulsive core in the interaction. Also mixed states are conceivable. In any case they should be antisymmetric with respect to particle exchange in order to include the Pauli principle from the very beginning. This accounts for the adjective "Fermionic".

The single particle states which enter into the many-body state are wave packets localized in phase-space, therefore the attribute "Molecular". They are the closest analogue to classical mechanics without violating the uncertainty principle.

For a chosen parametrization of the trial state the equations of motion for the parameters are derived from the time-dependent quantum variational principle. This principle constitutes the second building block, the "Dynamics". Since there is a unique mapping of the parameter set on the quantum trial state the dynamics of the parameters is actually the representation of the dynamics of the quantum many-body state. The derivation from a variational principle guarantees the proper conservation laws and leads to a generalized lagrangian dynamics on a symplectic manifold [15].

The third component is the hamiltonian of the system. The choice of the trial state depends of course crucially on the properties of the hamiltonian. In nuclear physics, the free two-body nucleon-nucleon interaction cannot be used directly in the many-body system. There are genuine many-body forces due to polarization of the nucleons and even more important, one needs effective interactions which are tailored to make up for deficiencies in the model state. Thus the choice of the trial state and the effective interaction are intimately related.

In the following subsections the model will be exemplified with a Slater determinant as trial state.

2.1 Time-dependent variational principle

The FMD model is based on the time-dependent variational principle

$$\delta \int_{t_1}^{t_2} dt \, \langle Q(t) | \, i\frac{d}{dt} - \underset{\sim}{H} \, | Q(t) \rangle \; = \; 0 \tag{1}$$

in which the trial state $\langle Q(t) |$ is to be varied. This many-body state is specified by a set of parameters $Q(t) = \{ \; q_\nu(t) \; | \; \nu = 1, 2, \cdots \}$ which are the generalized coordinates of the system.

The variation has to be performed with respect to each parameter $q_\nu(t)$ with the end points kept fixed, i.e. $\delta q_\nu(t_1) = \delta q_\nu(t_2) = 0$. The operator $\underset{\sim}{H}$ is the total hamiltonian of the system. (Throughout the paper operators in Hilbert space will be underlined with a twiddle, to distinguish them from parameters or expectation values.)

The Euler-Lagange equations

$$\frac{d}{dt}\frac{\partial \mathcal{L}}{\partial \dot{q}_\nu} - \frac{\partial \mathcal{L}}{\partial q_\nu} = 0 \qquad , \qquad \nu = 1, 2, \cdots, N \tag{2}$$

which result from the variation (1) are written in terms of the Lagrange function

$$\begin{aligned}\mathcal{L}\left(Q(t),\dot{Q}(t)\right) &:= \langle\, Q(t)\,|\; i\frac{d}{dt} - \underset{\sim}{H}\;|\, Q(t)\,\rangle \\ &= \mathcal{L}_0\left(Q(t),\dot{Q}(t)\right) \;-\; \mathcal{H}(Q(t))\;,\end{aligned} \tag{3}$$

with

$$\mathcal{L}_0\left(Q(t),\dot{Q}(t)\right) := \langle\, Q(t)\,|\, i\frac{d}{dt}\,|\, Q(t)\,\rangle = \sum_{\nu}\, \langle\, Q(t)\,|\; i\frac{\partial}{\partial q_\nu}\;|\, Q(t)\,\rangle\; \dot{q}_\nu\;, \tag{4}$$

in which $\dot{Q}(t) = \{\, \dot{q}_\nu \equiv dq_\nu/dt \mid \nu = 1, 2, \cdots \}$ is the set of generalized velocities and $\mathcal{H}(Q(t))$ is the Hamilton function defined as the expectation value of the hamiltonian $\underset{\sim}{H}$:

$$\mathcal{H}(Q(t)) = \langle\, Q(t)\,|\, \underset{\sim}{H}\,|\, Q(t)\,\rangle\;. \tag{5}$$

Different from classical mechanics the Lagrange function (3) is linear in the velocities $\dot{q}_\nu$ but at the same time the set $Q(t) = \{q_\nu(t)\}$ contains both, coordinates and momenta.

Using the general structure (3) of the Lagrange function the Euler-Lagrange equations (2) in their most general form can be written as

$$\sum_{\nu} \mathcal{A}_{\mu\nu}(Q)\; \dot{q}_\nu = -\frac{\partial}{\partial q_\mu}\mathcal{H}(Q) \tag{6}$$

or, if $\mathcal{A}_{\mu\nu}$ is not singular [16] the equations of motion are

$$\dot{q}_\mu = -\sum_{\nu} \mathcal{A}^{-1}_{\mu\nu}(Q)\; \frac{\partial}{\partial q_\nu}\mathcal{H}(Q)\;, \tag{7}$$

where

$$\mathcal{A}_{\mu\nu}(Q) = -\mathcal{A}_{\nu\mu}(Q) = \frac{\partial^2 \mathcal{L}_0}{\partial \dot{q}_\mu \partial q_\nu} - \frac{\partial^2 \mathcal{L}_0}{\partial \dot{q}_\nu \partial q_\mu}\;, \tag{8}$$

is a skew symmetric matrix, which depends in general on the variables $Q(t) = \{q_\nu(t)\}$. For details see section 2.5 and the appendix.

With help of the matrix $\mathcal{A}_{\mu\nu}$ one can define generalized Poisson brackets [17] as

$$\{\mathcal{H},\mathcal{B}\} := \sum_{\mu,\nu} \frac{\partial \mathcal{H}}{\partial q_\mu} \mathcal{A}^{-1}_{\mu\nu} \frac{\partial \mathcal{B}}{\partial q_\nu} , \tag{9}$$

such that the time derivative of an expectation value

$$\mathcal{B}(t) = \langle Q(t) \,|\, \underset{\sim}{B} \,|\, Q(t) \rangle \tag{10}$$

of a time-independent operator $\underset{\sim}{B}$ calculated with the trial state $|Q(t)\rangle$ is given by

$$\begin{aligned} \frac{d}{dt}\mathcal{B}(t) &= \frac{d}{dt}\langle Q(t) \,|\, \underset{\sim}{B} \,|\, Q(t) \rangle = \sum_\nu \dot{q}_\nu \frac{\partial}{\partial q_\nu}\mathcal{B} \\ &= \sum_{\mu,\nu} \frac{\partial \mathcal{H}}{\partial q_\mu} \mathcal{A}^{-1}_{\mu\nu} \frac{\partial \mathcal{B}}{\partial q_\nu} = \{\mathcal{H},\mathcal{B}\} \quad . \end{aligned} \tag{11}$$

Equation (11) has the symplectic manifold structure of hamiltonian dynamics [15], but in the general case the parameters q_ν cannot be grouped into pairs of canonical variables. However, according to Darboux's theorem canonical variables exist locally. They are non-linear functions of the parameters q_ν and have to be constructed such that $\mathcal{A}^{-1}_{\mu\nu}$ assumes the canonical form

$$\mathcal{A}^{-1}_{\mu\nu} = \begin{pmatrix} 0 & -E \\ E & 0 \end{pmatrix} , \tag{12}$$

where E is the unit matrix. Their choice, however, is not unique.

2.2 Conservation laws

After having solved the equations of motion (7) for the parameters $Q(t) = \{q_\nu(t) \mid \nu = 1,\cdots,NA\}$ the trial state $|Q(t)\rangle$ is known at all times. Thus one can calculate the expectation value $\mathcal{B}(t) = \langle Q(t) \,|\, \underset{\sim}{B} \,|\, Q(t) \rangle$ of an arbitrary time-independent operator $\underset{\sim}{B}$. With the definition (9) for the Poisson brackets the time derivative of this expectation value can be written as

$$\frac{d}{dt}\mathcal{B} = \{\mathcal{H},\mathcal{B}\} . \tag{13}$$

The expectation value is conserved in time if [18]

$$\{\mathcal{H},\mathcal{B}\} = \sum_{\mu,\nu} \frac{\partial \mathcal{H}}{\partial q_\mu}\, \mathcal{A}^{-1}_{\mu\nu}\, \frac{\partial \mathcal{B}}{\partial q_\nu} = 0 \tag{14}$$

Since $\mathcal{A}^{-1}_{\mu\nu}$ is skew symmetric the energy $\mathcal{H}$ itself is always conserved by the equations of motion, provided they are derived from the variational principle (1). This is completely independent on the choice of the trial state .

In the following we show with quite general considerations what other constants of motion are and how the trial state has to be chosen in order to ensure the desired conservation laws .

For that we consider a unitary transformation with the hermitean generator $\underset{\sim}{G}$

$$\underset{\sim}{U} = \exp\left(i\,\epsilon\,\underset{\sim}{G}\right) \quad , \quad \epsilon \quad \text{real} . \tag{15}$$

The following theorem is proven below.

Theorem: If $\underset{\sim}{U}$ maps the set of trial states onto itself

$$\underset{\sim}{U}\,|\,Q\,\rangle = |\,Q'\,\rangle \quad \in \quad \{\,|\,Q\,\rangle\} \ , \tag{16}$$

then, as a result of the equations of motion,

$$\begin{aligned} \frac{d}{dt}\mathcal{G} &= \{\mathcal{H},\mathcal{G}\} \\ = \frac{d}{dt}\langle\, Q(t)\,|\,\underset{\sim}{G}\,|\,Q(t)\,\rangle &= \langle\, Q(t)\,|\,i\left[\underset{\sim}{H},\underset{\sim}{G}\right]\,|\,Q(t)\,\rangle \ . \end{aligned} \tag{17}$$

That means that for this class of generators the generalized Poisson bracket is just the expectation value of the commutator with $i\underset{\sim}{H}$.

Proof: Since $\underset{\sim}{U}$ does not map out of the manifold of trial states a special variation of the trial state can be defined by a small time-dependent $\epsilon(t)$

$$\begin{aligned} |\,Q(t)+\delta Q(t)\,\rangle &= \exp\left(i\epsilon(t)\underset{\sim}{G}\right)\,|\,Q(t)\,\rangle \\ &= (1+i\epsilon(t)\underset{\sim}{G})\,|\,Q(t)\,\rangle \ + \ O(\epsilon^2) \ . \end{aligned} \tag{18}$$

Inserting this into the variational principle yields

$$
\begin{aligned}
0 &= \int_{t_1}^{t_2} dt \left\{ \langle Q(t) + \delta Q(t) \,|\, i\frac{d}{dt} - \underset{\sim}{H} \,|\, Q(t) + \delta Q(t) \rangle - \langle Q(t) \,|\, i\frac{d}{dt} - \underset{\sim}{H} \,|\, Q(t) \rangle \right\} \\
&= \int_{t_1}^{t_2} dt \left\{ \epsilon(t) \langle Q(t) \,|\, i \left[\underset{\sim}{G}, \underset{\sim}{H} \right] \,|\, Q(t) \rangle - \langle Q(t) \,|\, \dot{\epsilon}(t) \underset{\sim}{G} \,|\, Q(t) \rangle \right\} \\
&= \int_{t_1}^{t_2} dt \; \epsilon(t) \; \left\{ \langle Q(t) \,|\, i \left[\underset{\sim}{G}, \underset{\sim}{H} \right] \,|\, Q(t) \rangle + \frac{d}{dt} \langle Q(t) \,|\, \underset{\sim}{G} \,|\, Q(t) \rangle \right\} \\
&\quad - \int_{t_1}^{t_2} d\langle Q(t) \,|\, \epsilon(t) \underset{\sim}{G} \,|\, Q(t) \rangle \; . \qquad (19)
\end{aligned}
$$

The last intregral vanishes because $\epsilon(t_1) = \epsilon(t_2) = 0$. But otherwise the variation $\epsilon(t)$ is arbitrary so that the integral can be zero only if eq. (17) is fulfilled, q.e.d.

Relation (17) is very useful for two reasons. First, if $\underset{\sim}{G}$ commutes with the hamiltonian $\underset{\sim}{H}$ and $\exp(i\varepsilon \underset{\sim}{G}) \,|\, Q \rangle = |\, Q' \rangle$ then $\langle Q(t) \,|\, \underset{\sim}{G} \,|\, Q(t) \rangle$ is automatically a constant of motion.

Second, this relation is an important guidance for the choice of the trial state $|\, Q \rangle$. If one wants the model to obey certain conservation laws then the set of trial states should be invariant under the unitary transformations generated by the constants of motion. For example total momentum conservation implies that a translated trial state is again a valid trial state. This is fulfilled for the trial states which will be specified in the following section 2.3. The gaussians defined in eq. (23) can be translated or Galilei boosted, the latter taking care of the conservation of the centre of gravity.

Conservation of total spin $\underset{\sim}{\boldsymbol{J}} = \underset{\sim}{\boldsymbol{L}} + \underset{\sim}{\boldsymbol{S}}$ is guaranteed when rotation of the trial state in coordinate and spin space results again in a trial state. This implies that the gaussian (23) has to have either a spherical shape or the width parameter has to be replaced by a complete tensor with 12 real parameters. It also means that all spin directions in $|\, \phi, \chi \rangle$ have to be allowed.

Relation (17) establishes also a connection to Ehrenfest's theorem and sheds some light on the quality of the variational principle (1). It says that under the premises that $\exp(i\varepsilon \underset{\sim}{G})$ does not map out of the set of trial states the expectation value of $\underset{\sim}{G}$ develops for short times $(t - t_0)$ like the exact solution. From eq. (17) follows that

$$
\frac{d}{dt}(\mathcal{G}(t) - \mathcal{G}_{exact}(t)) = 0 \; , \qquad (20)
$$

where the exact solution with the initial state $|Q(t_0)\rangle$ is

$$\mathcal{G}_{exact}(t) = \langle Q(t_0)|\, e^{i(t-t_0)\underset{\sim}{H}}\, \underset{\sim}{G}\, e^{-i(t-t_0)\underset{\sim}{H}}\, |Q(t_0)\rangle\ . \tag{21}$$

The kinetic energy $\underset{\sim}{T}$ is such a generator. Since our trial state (30) is the exact solution of the Schrödinger equation without interactions it fulfills

$$\exp(-i\tau\underset{\sim}{T})\,|Q(t)\rangle = |Q(t+\tau)\rangle\ . \tag{22}$$

With the two-body interaction included, $|Q(t)\rangle$ is not an exact solution anymore, but the expectation value of the total kinetic energy, which then is not a conserved quantity any longer, is well approximated in the sense of eq. (20).

2.3 Trial state

Classical molecular dynamics describes the physical system by Newton's equations of motion for a set of centre-of-mass coordinates of molecules which interact with each other via two-body interactions. These interactions are usually repulsive at short and attractive at longer distances.

Instead of classical points in phase space FMD deals with wave packets which are localized in phase space. For each nucleon (molecule) there is a gaussian wave packet parametrized by the set $q(t) = \{\boldsymbol{r}(t), \boldsymbol{p}(t), a(t), \chi(t), \phi(t), \xi\}$

$$\langle \boldsymbol{x}\,|\,q(t)\rangle = \exp\left\{ -\frac{(\boldsymbol{x}-\boldsymbol{r}(t))^2}{2\,a(t)} + i\boldsymbol{p}(t)\boldsymbol{x} + i\eta(t)\right\} \otimes |\,\chi(t),\phi(t)\rangle \otimes |\,\xi\rangle\ , \tag{23}$$

which in quantum mechanics is the closest analogue to a classical particle described by a single point in phase-space. $\eta(t)$ is a complex parameter which contains the phase and the norm.

In FMD the match to classical positions and momenta are the parameters $\boldsymbol{r}(t)$ and $\boldsymbol{p}(t)$ which determine the mean values of the position and momentum operator of the single particle state

$$\boldsymbol{r}(t) = \frac{\langle q(t)\,|\,\underset{\sim}{\boldsymbol{x}}\,|\,q(t)\rangle}{\langle q(t)\,|\,q(t)\rangle}\quad ,\quad \boldsymbol{p}(t) = \frac{\langle q(t)\,|\,\underset{\sim}{\boldsymbol{k}}\,|\,q(t)\rangle}{\langle q(t)\,|\,q(t)\rangle}\ . \tag{24}$$

Due to the quantum mechanical uncertainty relation the wave packet can be either narrow in coordinate space and wide in momentum space or vice versa. This non-classical degree of freedom is taken care of by the complex width

parameter $a(t) = a_R(t) + ia_I(t)$. It determines via its real part $a_R(t)$ the variance of the momentum distribution by the relation

$$\frac{3}{2a_R(t)} = \frac{\langle q(t) \,|\, (\underset{\sim}{k} - \boldsymbol{p}(t))^2 \,|\, q(t) \rangle}{\langle q(t) \,|\, q(t) \rangle} = 3\sigma_K^2(t) \; . \tag{25}$$

Since the wave packet is spherical the widths are equal in all three cartesian directions. The imaginary part $a_I(t)$ appears in the expression for the spatial width as

$$\frac{3}{2} \frac{a_R^2(t) + a_I^2(t)}{a_R(t)} = \frac{\langle q(t) \,|\, (\underset{\sim}{x} - \boldsymbol{r}(t))^2 \,|\, q(t) \rangle}{\langle q(t) \,|\, q(t) \rangle} = 3\sigma_X^2(t) \tag{26}$$

and determines in how far the wave packet is of minimal uncertainty. The product of the variances

$$\sigma_X^2 \; \sigma_K^2 = \frac{1}{4} \left(1 + \frac{a_I^2}{a_R^2} \right) \tag{27}$$

shows that for $a_I = 0$ one has the minimum-uncertainty packet where $\sigma_X \sigma_K = \frac{1}{2}$, while for $a_I \neq 0$ the uncertainty can become arbitrarily large. This means that the particle occupies more than $(\hbar/2\pi)^3$ of phase space volume but at a lower phase space density, such that other fermions can find place at the same area in phase space.

Besides the parameters for the spatial part of the wave packet there are two parameters $\chi(t)$ and $\phi(t)$ for the spin degree of freedom. If one parametrizes the trial spin state by

$$\langle m_s \,|\, \chi(t), \phi(t) \rangle = \begin{cases} \cos \frac{\chi(t)}{2} & : \quad m_s = \frac{1}{2} \\ \sin \frac{\chi(t)}{2} \, \mathrm{e}^{i\phi(t)} & : \quad m_s = -\frac{1}{2} \end{cases} \; , \tag{28}$$

the relation between the parameters and the corresponding spin operators is

$$\boldsymbol{\sigma}(t) = \frac{\langle q(t) \,|\, \underset{\sim}{\boldsymbol{\sigma}} \,|\, q(t) \rangle}{\langle q(t) \,|\, q(t) \rangle} \; , \tag{29}$$

where $\boldsymbol{\sigma}(t) = (\sin\chi(t)\cos\phi(t), \sin\chi(t)\sin\phi(t), \cos\chi(t))$ is a vector in the 3-dimensional real space and the quantization axis is the 3-axis. Thus $\boldsymbol{\sigma}(t)$ can be regarded as the "classical" spin direction just like $\boldsymbol{r}(t)$ or $\boldsymbol{p}(t)$, although there is no classical spin degree of freedom which can vary only its direction but not its magnitude as it is the case for $\boldsymbol{\sigma}(t)$.

In principle the same parametrization can be chosen for the isospin part $|\xi\rangle$. A time-dependent isospin would mean that for example due to the exchange of charged pions neutrons can dynamically transform into protons and vice versa. In this paper we shall not consider rotations in isospin space but $|\xi\rangle$ is assumed to be independent of time and either $|\xi\rangle = |proton\rangle$ or $|\xi\rangle = |neutron\rangle$.

To describe a system with A fermions we construct with these parametrized single-particle states $|q_k(t)\rangle$ a Slater determinant

$$|q_1(t), q_2(t), \cdots, q_A(t)\rangle \equiv |Q(t)\rangle = \frac{1}{\langle \widehat{Q(t)} | \widehat{Q(t)} \rangle^{\frac{1}{2}}} \; |\widehat{Q(t)}\rangle \; , \tag{30}$$

where the antisymmetrized but not normalized state $|\widehat{Q(t)}\rangle$ is given by

$$|\widehat{Q(t)}\rangle = \frac{1}{A!} \sum_{all\ P} \mathrm{sgn}(P) \; |q_{P(1)}(t)\rangle \otimes |q_{P(2)}(t)\rangle \otimes \cdots \otimes |q_{P(A)}(t)\rangle \; . \tag{31}$$

The sum runs over all permutations P and $\mathrm{sgn}(P)$ is the sign of the permutation. It should be noted that $q_k(t) = \{\boldsymbol{r}_k(t), \boldsymbol{p}_k(t), a_k(t), \chi_k(t), \phi_k(t), \xi_k\}$ denotes the set of parameters specifying the single-particle state with number k. The parameter set for the many-body state thus reads

$$\begin{aligned} Q(t) &= \{\boldsymbol{r}_1(t), \boldsymbol{p}_1(t), a_1(t), \chi_1(t), \phi_1(t), \xi_1; \boldsymbol{r}_2(t), \cdots; \boldsymbol{r}_3(t), \cdots, \xi_A\} \\ &= \{q_\nu(t) \mid \nu = 1, \cdots, \mathrm{N}A\} \; , \end{aligned} \tag{32}$$

where N is the number of real parameters per particle, in our case N=10. Whenever q carries a greek index it is a parameter, whereas a latin index implies that q_k is the whole set for the state $|q_k\rangle$.

Due to antisymmetrization FMD is constrained to the antisymmetric subspace of the Hilbert space and hence the Pauli principle is a priori incorporated. Furthermore, the projection (31) from a product state onto the antisymmetric subspace destroys for overlapping gaussians the localization of the particles and introduces shell model states. This will be discussed and explicitly shown in section 3.2. If the single-particle states $|q_k\rangle$ are not overlapping, the antisymmetrization has no effect anymore and the particles are localized in the individual wave packets. In this limit we return to classical newtonian mechanics for $\boldsymbol{r}_k(t)$ and $\boldsymbol{p}_k(t)$, which however can still be coupled to the non-classical variables $\boldsymbol{\sigma}_l(t)$ for the spin directions and the widths $a_l(t)$. Of course also in this limit the particles are indistinguishable and it is not possible to decide which particle occupies which gaussian packet.

2.4 *Expectation values of one- and two-body operators*

In the FMD model we encounter one- and two-body operators for which expectation values have to be calculated with the FMD trial states. Since the single-particle states are not orthogonal the expressions involve overlap matrices [23].

The norm of the many-body trial state is given by

$$\begin{aligned} \langle \widehat{Q(t)} \,|\, \widehat{Q(t)} \rangle &= \{ \langle q_1(t) | \otimes \cdots \otimes \langle q_A | \} \; | \widehat{Q(t)} \rangle \\ &= \frac{1}{A!} \det \left(\; \{ \langle q_k(t) \,|\, q_l(t) \rangle \} \; \right) \end{aligned} \tag{33}$$

with the single particle overlaps $\langle q_k(t) \,|\, q_l(t) \rangle$ given in Appendix A.1.

The matrix $\mathcal{O}_{kl}$ which will appear often in the following expressions is defined as the inverse of the overlap matrix $\langle q_k(t) \,|\, q_l(t) \rangle$

$$\left(\mathcal{O}^{-1} \right)_{kl} (t) := \langle q_k(t) \,|\, q_l(t) \rangle \; ; \quad k,l = 1, \cdots, A \; . \tag{34}$$

In the following the time dependence will not always be indicated explicitly.

If the many-body trial state is a single Slater determinant all expectation values can be calculated with the one-body density matrix

$$\underset{\sim}{\varrho}^{(1)} = \sum_{k,l=1}^{A} | q_k \rangle \; \mathcal{O}_{kl} \; \langle q_l | \; . \tag{35}$$

It is easy to verify that $\underset{\sim}{\varrho}^{(1)}$ is a projection operator

$$(\underset{\sim}{\varrho}^{(1)})^\dagger = \underset{\sim}{\varrho}^{(1)} \quad \text{and} \quad (\underset{\sim}{\varrho}^{(1)})^2 = \underset{\sim}{\varrho}^{(1)} \; , \tag{36}$$

which implies that the occupation numbers are either 0 or 1. The non-orthogonal gaussians $| q_m \rangle$ are eigenstates of $\underset{\sim}{\varrho}^{(1)}$ with eigenvalues 1. An orthonormal set of eigenfunctions will be given in section 3.2 where the relation to the shell model is discussed.

The expectation value of a one-body operator $\underset{\sim}{T}$ is conveniently calculated with $\underset{\sim}{\varrho}^{(1)}$ as

$$\langle Q \,|\, \underset{\sim}{T} \,|\, Q \rangle = \mathrm{tr} \left(\underset{\sim}{\varrho}^{(1)} \underset{\sim}{t} \right) = \sum_{k,l=1}^{A} \langle q_k \,|\, \underset{\sim}{t} \,|\, q_l \rangle \; \mathcal{O}_{lk} \; . \tag{37}$$

Small letters underlined by a tilde, like $\underset{\sim}{t}$ for the kinetic energy, denote operators in one-body space while capital letters, here $\underset{\sim}{T}$, represent the operators in the A-body space.

For a single Slater determinant the two-body density $\underset{\sim}{\rho}^{(2)}$ can be expressed solely in terms of $\underset{\sim}{\rho}^{(1)}$ as

$$\underset{\sim}{\rho}^{(2)} = \frac{1}{4} \sum_{k,l,m,n=1}^{A} |\, q_k, q_l \,\rangle_a \; \mathcal{O}_{km}\mathcal{O}_{ln} \; {}_a\langle\, q_m, q_n \,| \;, \tag{38}$$

where two-body states and antisymmetrized two-body states are denoted by

$$|\, q_m, q_n \,\rangle := |\, q_m \,\rangle \otimes |\, q_n \,\rangle \quad \text{and} \tag{39}$$

$$|\, q_m, q_n \,\rangle_a := |\, q_m \,\rangle \otimes |\, q_n \,\rangle \; - \; |\, q_n \,\rangle \otimes |\, q_m \,\rangle \;, \tag{40}$$

respectively. Thus the expectation value of a two-body operator $\underset{\sim}{V}$ is given by

$$\begin{aligned} \langle\, Q \,|\, \underset{\sim}{V} \,|\, Q \,\rangle &= \mathrm{tr}\left(\underset{\sim}{\rho}^{(2)} \underset{\sim}{v}\right) \\ &= \frac{1}{2} \sum_{k,l,m,n=1}^{A} \langle\, q_m, q_n \,|\, \underset{\sim}{v} \,|\, q_k, q_l \,\rangle_a \; \mathcal{O}_{km}\mathcal{O}_{ln} \;. \end{aligned} \tag{41}$$

In the case of two-body operators small letters underlined by a tilde, like $\underset{\sim}{v}$, denote operators in the two-body space, while capital letters represent the same operators in A-body space.

2.5 Equations of motion for FMD

In this section the more general discussion on the time-dependent variational principle and the resulting equations of motion will be exemplified with the trial state of FMD defined in section 2.3.

Since the hamiltonian $\underset{\sim}{H}$ used in FMD contains the kinetic energy $\underset{\sim}{T}$ and the two-body interaction $\underset{\sim}{V}$ the Lagrange function is split into three parts

$$\mathcal{L}(Q, \dot{Q}) = \mathcal{L}_0(Q, \dot{Q}) - \mathcal{T}(Q) - \mathcal{V}(Q) \;, \tag{42}$$

where $\mathcal{L}_0(Q, \dot{Q})$ is defined in eq. (4) and the hamilton function is according to $\underset{\sim}{H} = \underset{\sim}{T} + \underset{\sim}{V}$ decomposed into

$$\mathcal{H}(Q) = \langle Q(t) \,|\, \underset{\sim}{H} \,|\, Q(t) \rangle = \mathcal{T}(Q) + \mathcal{V}(Q) \tag{43}$$

with

$$\mathcal{T}(Q) := \langle Q(t) \,|\, \underset{\sim}{T} \,|\, Q(t) \rangle \quad \text{and} \tag{44}$$

$$\mathcal{V}(Q) := \langle Q(t) \,|\, \underset{\sim}{V} \,|\, Q(t) \rangle \; . \tag{45}$$

The time derivatives of the parameters $\dot{q}_\nu$ appear only in $\mathcal{L}_0$. Furthermore, $\mathcal{L}_0$ is linear in $\dot{q}_\nu$ so that the Euler-Lagrange equations (2) can be written as

$$\frac{d}{dt}\left(\frac{\partial \mathcal{L}_0}{\partial \dot{q}_\mu}\right) - \frac{\partial \mathcal{L}_0}{\partial q_\mu} = \sum_\nu \mathcal{A}_{\mu\nu}\, \dot{q}_\nu = -\frac{\partial \mathcal{T}}{\partial q_\mu} - \frac{\partial \mathcal{V}}{\partial q_\mu} \; , \tag{46}$$

where the skew symmetric matrix $\mathcal{A}_{\mu\nu}$, which takes care of the geometrical properties of the manifold of trial states, is given by

$$\begin{aligned} \mathcal{A}_{\mu\nu} &:= \frac{\partial^2 \mathcal{L}_0}{\partial \dot{q}_\mu \partial q_\nu} - \frac{\partial^2 \mathcal{L}_0}{\partial \dot{q}_\nu \partial q_\mu} = 2\,\mathrm{Im}\,\langle \frac{\partial}{\partial q_\mu} Q(t) \,|\, \frac{\partial}{\partial q_\nu} Q(t) \rangle \\ &= 2\,\mathrm{Im}\left\{ \left[\langle \frac{\partial}{\partial q_\mu} q_m \,|\, \frac{\partial}{\partial q_\nu} q_n \rangle - \sum_{r,s=1}^{A} \langle \frac{\partial}{\partial q_\mu} q_m \,|\, q_r \rangle\, \mathcal{O}_{rs}\, \langle q_s \,|\, \frac{\partial}{\partial q_\nu} q_n \rangle \right] \mathcal{O}_{nm} \right\} . \end{aligned} \tag{47}$$

The greek subscripts $\mu = \{m, i\}$ and $\nu = \{n, j\}$ represent two indices; n and m are the numbers of the wave packets, while i and j label the parameters for each packet. The detailed derivation of $\mathcal{A}_{\mu\nu}$ is given in appendix A.2.

Using the permutation symmetries and the hermiticity of $\underset{\sim}{T}$ and $\underset{\sim}{V}$ (as shown in appendix A.1 and A.2) the generalized forces can be written as

$$\mathcal{F}_\mu = -\frac{\partial}{\partial q_\mu}\mathcal{H} = -\frac{\partial}{\partial q_\mu}\mathcal{T} - \frac{\partial}{\partial q_\mu}\mathcal{V} \tag{48}$$

with

$$\begin{aligned} \frac{\partial}{\partial q_\mu}\mathcal{T} &= \mathrm{tr}\left(\frac{\partial \underset{\sim}{\rho}^{(1)}}{\partial q_\mu}\, \underset{\sim}{t} \right) \\ &= 2\,\mathrm{Re} \sum_{k=1}^{A} \left[\langle \frac{\partial}{\partial q_\mu} q_m \,|\, \underset{\sim}{t} \,|\, q_k \rangle - \sum_{r,s=1}^{A} \langle \frac{\partial}{\partial q_\mu} q_m \,|\, q_r \rangle\, \mathcal{O}_{rs}\, \langle q_s \,|\, \underset{\sim}{t} \,|\, q_k \rangle \right] \mathcal{O}_{km} \; . \end{aligned} \tag{49}$$

The contribution of the two-body interaction to the generalized force is given

by

$$\frac{\partial}{\partial q_\mu}\mathcal{V} = \mathrm{tr}\left(\frac{\partial \underset{\sim}{\rho}^{(2)}}{\partial q_\mu}\,\underset{\sim}{v}\right)$$
$$= 2\,\mathrm{Re}\sum_{k,l,n=1}^{A}\Bigg[\langle\frac{\partial}{\partial q_\mu}q_m, q_n \,|\, \underset{\sim}{v} \,|\, q_k, q_l\rangle_a \qquad (50)$$
$$- \sum_{r,s=1}^{A}\langle\frac{\partial}{\partial q_\mu}q_m \,|\, q_r\rangle\,\mathcal{O}_{rs}\,\langle q_s, q_n \,|\, \underset{\sim}{v} \,|\, q_k, q_l\rangle_a\Bigg]\,\mathcal{O}_{km}\,\mathcal{O}_{ln}\ .$$

The derivative of a two-particle product state is defined by

$$\langle\frac{\partial}{\partial q_\mu}q_m\,, q_n| \;:=\; \left(\frac{\partial}{\partial q_\mu}\langle q_m|\right)\otimes\langle q_n|\ , \qquad (51)$$

where the derivative $\partial/\partial q_\mu$ acts only on the state $\langle q_m|$. The derivatives of the matrix elements are given in appendix A.3.

It should be noted that, due to the fact that the kinetic energy $\underset{\sim}{T}$ is a generator for a unitary transformation which does not map out of the manifold of the trial states, $\sum_\nu \mathcal{A}^{-1}_{\mu\nu}\frac{\partial \mathcal{T}}{\partial q_\nu}$ assumes a very simple form:

$$-\sum_{\nu=1}^{AN}\mathcal{A}^{-1}_{\mu\nu}\frac{\partial \mathcal{T}}{\partial q_\nu} = \begin{cases} \boldsymbol{p}_m/m_N & \text{for} \quad \dot{\boldsymbol{r}}_m \\ 1/m_N & \text{for} \quad \dot{a}_{Im} \\ 0 & \text{for} \quad \text{all other velocities} \end{cases}, \qquad (52)$$

m_N being the mass of the nucleons.

3 Numerical results

3.1 Two-body interactions and ground states

Up to now the interaction $\underset{\sim}{V}$ contained in the hamiltonian was not specified. Since in this paper we shall only investigate nuclei with a few nucleons, we adopt two-body potentials which have been successfully used for the description of small nuclei [19,20]. These interactions are repulsive at small and attractive at larger distances. The repulsive core is, however, rather weak and one should regard the potentials as a phenomenological ansatz for a G-matrix rather than the free nucleon-nucleon interaction which has a very strong repulsion for distances smaller than 0.5 fm. In this paper we are using potentials of the form

$$\begin{aligned}\underset{\sim}{V}(i,j) = &\left(w_a + (1-w_a)\,\underset{\sim}{P}^M(i,j)\right)\,\underset{\sim}{V}_a(i,j) \\ &+\left(w_r + (1-w_r)\,\underset{\sim}{P}^M(i,j)\right)\,\underset{\sim}{V}_r(i,j)\;,\end{aligned} \tag{53}$$

where $\underset{\sim}{P}^M(i,j)$ denotes the Majorana exchange of the spatial coordinates. The radial dependences are of gaussian type given by

$$\begin{aligned}\langle\, \boldsymbol{x}_i, \boldsymbol{x}_j \,|\, \underset{\sim}{V}_{r,a}(1,2) \,|\, \boldsymbol{x}_k, \boldsymbol{x}_l \,\rangle \quad &= \\ V_{r,a}\;\delta^3(\boldsymbol{x}_i - \boldsymbol{x}_k)\,\delta^3(\boldsymbol{x}_j - \boldsymbol{x}_l)\;&\exp\left\{-\frac{(\boldsymbol{x}_i - \boldsymbol{x}_j)^2}{r_{r,a}^2}\right\},\end{aligned} \tag{54}$$

which allows to calculate all matrix elements and their derivatives analytically. Altogether we used four interactions, denoted by B1 and C1 which are taken from Brink and Boeker [20], and V1 and V2 taken from Volkov [19]. The parameters are summarized in table 1.

Since this paper deals only with small nuclei the Coulomb interaction is not included in the dynamics.

In FMD the ground state of a nucleus is the many-body state $|\,Q_{GS}\,\rangle$ in which the total energy $\mathcal{H} = \langle\, Q_{GS} \,|\, \underset{\sim}{H} \,|\, Q_{GS}\,\rangle$ is an absolute minimum with respect to variation of all parameters q_ν,

$$\frac{\partial}{\partial q_\nu}\,\mathcal{H} = 0\;. \tag{55}$$

This implies that the FMD ground state is completely time-independent (up to an overall phase) and the time derivatives of all parameters vanish because,

	w_a	V_a/MeV	r_a/fm	w_r	V_r/MeV	r_r/fm
B1	0.5136	-140.6	1.4	1.529	389.5	0.7
C1	0.6185	-117.4	1.4	2.635	271.0	0.7
V1	0.4	-83.34	1.6	0.4	144.86	0.82
V2	0.4	-60.65	1.8	0.4	61.15	1.01

Table 1
Parameters of the two–body interaction taken from ref. [20] and [19]

by definition, all generalized forces $\partial\mathcal{H}/\partial q_\mu$ are zero and hence

$$\dot{q}_\nu = -\sum_\mu \mathcal{A}^{-1}_{\nu\mu} \frac{\partial \mathcal{H}}{\partial q_\mu} = 0 \ . \tag{56}$$

Requirement (55) not only determines the positions $\boldsymbol{r}_k$ and momenta $\boldsymbol{p}_k$ but also the complex widths a_k and the spin directions (χ_k, ϕ_k).

Besides the ground state energy we calculate also the root-mean-square radius of the charge distribution. Before comparing with experimental data we subtract from both the contribution of the centre-of-mass motion and add the Coulomb energy

$$E_{GS} = \langle\, Q_{GS} \,|\, \underset{\sim}{H} \,|\, Q_{GS} \,\rangle - \langle\, Q_{GS} \,|\, \frac{1}{2\,A\,m_N} \underset{\sim}{\boldsymbol{K}}^2_{CM} \,|\, Q_{GS} \,\rangle + E_C \tag{57}$$

$$R^2_{rms} = \frac{1}{Z} \sum_{i=1}^{A} \langle\, Q_{GS} \,|\, (\underset{\sim}{\boldsymbol{X}}(i) - \underset{\sim}{\boldsymbol{X}}_{CM})^2 \underset{\sim}{P}^p(i) \,|\, Q_{GS} \,\rangle + R^2_{proton} \ , \tag{58}$$

where the total centre-of-mass momentum operator $\underset{\sim}{\boldsymbol{K}}_{CM}$ is the sum of single particle momenta

$$\underset{\sim}{\boldsymbol{K}}_{CM} = \sum_{i=1}^{A} \underset{\sim}{\boldsymbol{K}}(i) \tag{59}$$

and the centre-of-mass position operator is

$$\underset{\sim}{\boldsymbol{X}}_{CM} = \frac{1}{A} \sum_{i=1}^{A} \underset{\sim}{\boldsymbol{X}}(i) \ . \tag{60}$$

The operator $\underset{\sim}{P}^p(i)$ projects on protons and $R^2_{proton} = 0.876$ fm takes the finite

	^{4}He		^{6}Li		^{7}Li	
	E_{GS}/MeV	R_{rms}/fm	E_{GS}/MeV	R_{rms}/fm	E_{GS}/MeV	R_{rms}/fm
B1	-25.73	1.87	-14.61	2.52	-10.39	2.58
C1	-25.25	1.81	-11.88	2.50	-7.30	2.57
V1	-25.12	1.87	-15.65	2.45	-11.71	2.49
V2	-25.87	1.88	-17.30	2.47	-13.74	2.52
Exp.	-28.30	1.67	-31.99	2.50	-39.24	2.39
	^{8}Be		^{12}C		^{16}O	
	E_{GS}/MeV	R_{rms}/fm	E_{GS}/MeV	R_{rms}/fm	E_{GS}/MeV	R_{rms}/fm
B1	-40.25	2.72	-57.43	2.84	-88.40	2.77
C1	-38.70	2.64	-54.91	2.78	-81.25	2.73
V1	-40.88	2.55	-65.28	2.47	-122.77	2.38
V2	-43.79	2.55	-71.86	2.46	-134.74	2.34
Exp.	-56.50		-92.16	2.46	-127.62	2.73

Table 2
Groundstate energies and charge radii in FMD for various nuclei and different interactions [23]. The experimental mass defects are taken from ref. [21] and the charge radii from ref. [22]. All experimental errors are at most in the last digit.

charge radius of the proton into account. The Coulomb energy E_C is estimated from the charge radius by

$$E_C = \sqrt{\frac{3}{8}}\,\frac{Z(Z-1)e^2}{R_{rms}}\,, \tag{61}$$

which is appropriate for gaussian distributions.

We also determined the ground states by minimizing the expectation value of the hamiltionian minus the centre-of-mass energy as defined in eq. (57). This is preferable for the comparision with experimental ground state data. But the so found states cannot be used in a dynamical evolution with the hamiltonian $\mathcal{H}$ as they would not be stationary. Anyhow, the differences are not essential and decrease with mass number A.

For the ^{4}He case our results should coincide with the original work of Volkov [19] and Brink and Boeker [20] because our trial state is the same as the ground state of an harmonic oscillator which they used. While the energies

could be reproduced within three digits, the width parameter we obtained is the same as in the Brink and Boeker publication but differs from the numbers given by Volkov.

Since in the dynamical calculation we do not correct for the centre-of-mass motion we also use the ground states of the hamiltonian without correction.

In table 2 we summarize the ground state binding energies and charge radii. A surprising result was that for ^{8}Be and ^{12}C the FMD trial state gives more binding then the Hartree-Fock state used by Brink and Boeker which was a superposition of harmonic oscillator shells. This means that the localized gaussians are closer to the exact Hartree-Fock ground state then the restricted harmonic oscillator basis used by Brink and Boeker.

In fig. 1 and 2 we display for the V2 interaction, which compares most favourably with the measured masses, the density of different ground states in coordinate and momentum space, respectively. They are defined as

$$\rho_x(\boldsymbol{x}) = \langle \boldsymbol{x} \,|\, \underset{\sim}{\rho}^{(1)} \,|\, \boldsymbol{x} \rangle \quad \text{and} \quad \rho_k(\boldsymbol{k}) = \langle \boldsymbol{k} \,|\, \underset{\sim}{\rho}^{(1)} \,|\, \boldsymbol{k} \rangle \,, \tag{62}$$

where $\underset{\sim}{\rho}^{(1)}$ is the one-body density matrix given in eq. (35). The crosses in-

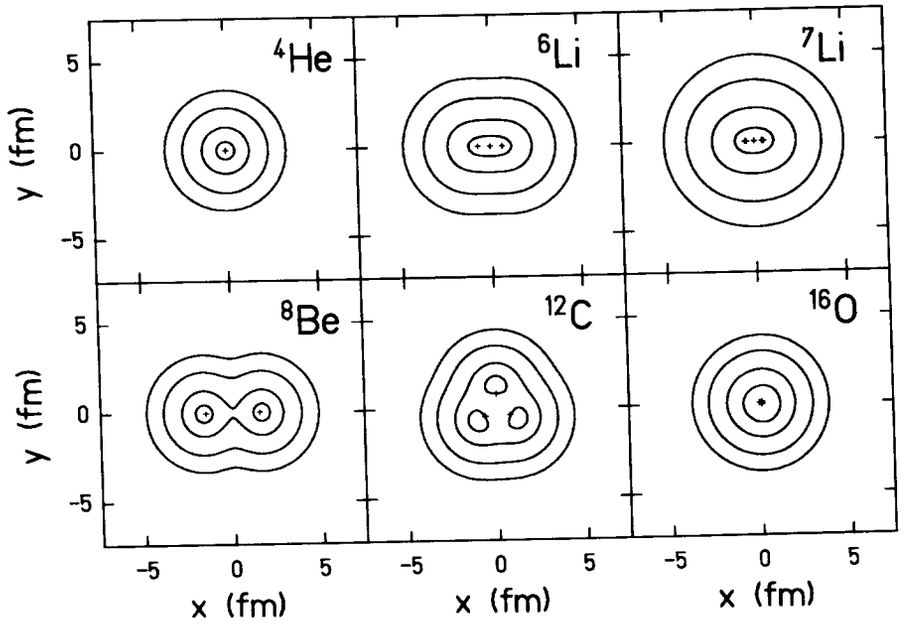

Fig. 1. Contour plot of spatial densities integrated over z-direction for different ground states. Crosses indicate centroids of wave packets. Contour lines are at 0.9, 0.5, 0.1 and 0.001 of maximum density.

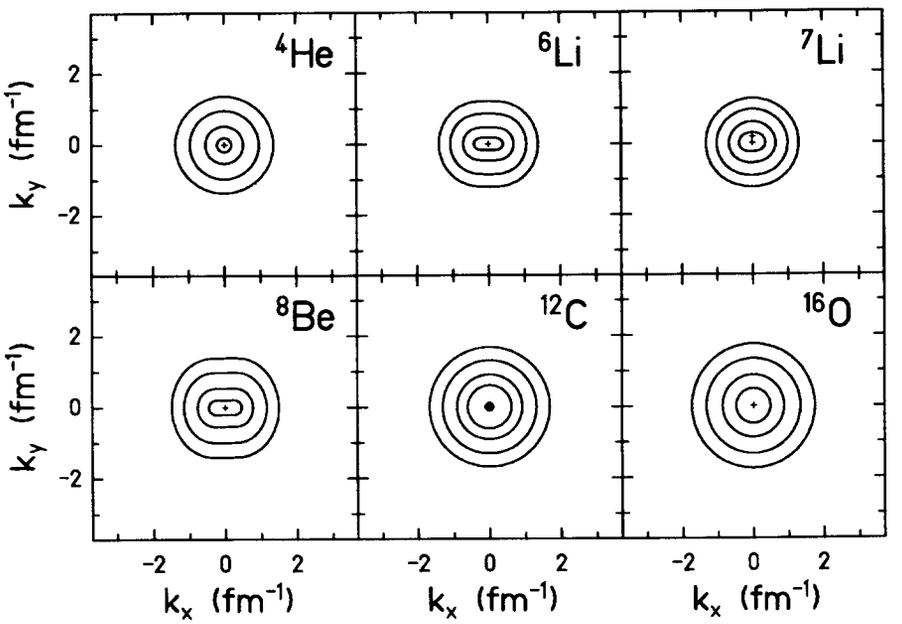

Fig. 2. Contour plot of momentum distributions integrated over z-direction for different ground states. Crosses indicate centroids of wave packets. Contour lines are at 0.9, 0.5, 0.1 and 0.001 of maximum density.

dicate the centres $\boldsymbol{r}_k$ and $\boldsymbol{p}_k$ of the wave packets and the densities shown are integrated over the z-direction. In ^{4}He all four wave-packets sit on top of each other because the different spins and isospins of the four nucleons allow a coordinate-space part of the four particle state which is symmetric under permutations.

Adding a proton and a neutron leads to ^{6}Li in which now two proton and two neutron wave-packets are moved a little out of the centre so that two nucleons with equal spin do not occupy the same s-state anymore, rather a p-state can be formed out of two neighbouring gaussians (see section 3.2). This p-state, which is oriented along the x-axis, contains higher momenta as can be seen in the corresponding momentum distribution which is elongated in k_x direction. Without antisymmetrization the momentum distribution would be spherical since all mean momenta $\boldsymbol{p}_k$ are at zero. The next neutron in ^{7}Li arranges itself at zero in coordinate space, but at a non-zero mean momentum (see fig. 2) shifting the mean positions of the other neutrons a little. The ^{8}Be nucleus turns out to be a loosely bound pair of α-particles (the barrier in the FMD calculation is less than 6 MeV). In nature ^{8}Be decays with a life time of $7 \cdot 10^{-17}$s into two α-particles.

In ^{12}C three α-particles are arranged in a triangle. The dominance of the α-cluster structure is typical for the V2 interaction because it contains only a Marojana exchange which makes an α-particle well bound and conserves the α-symmetry.

Different from ^{12}C the ground state of ^{16}O consists of 16 packets which are all centred at $\boldsymbol{x}_k = 0$ and $\boldsymbol{p}_k = 0$. There is still a tiny displacement in cordinate space which is a numerical effect because otherwise the antisymmetrization would project onto zero. The reason is that ^{16}O is a doubly magic nucleus which is spherical. Taking into account, that a Slater determinant, up to a phase, is invariant under unitary transformations of the occupied states, it is easy to realize that linear combinations of 16 gaussians sitting very close result in a perfect shell model state, in which the s- and p-states are completely filled. In the following section 3.2 we show with help of two examples how the shell structure enters the FMD trial state.

In FMD the Fermi motion is a quantum mechanical zero-point motion which resides to a large extent in the widths of the wave packets. But also the antisymmetrization is essential as for example in ^{6}Li or ^{8}Be it builds deformed distributions out of spherical packets. Fermi motion is not a random motion of the packet centroids. In the ground state $\boldsymbol{r}_k$ and $\boldsymbol{p}_k$ and all other parameters are time-independent otherwise it would be not the ground state of the system.

Models like QMD simulate the Fermi distribution by random motion of the centroids [6] which represents actually an excited model state. Therefore, in such models a special choice for initializing this motion must be found in order to prepare a system which does not cool already by evaporating particles before the collision takes place. For the same reason the study of outcoming fragments is strongly handicapped in models which do not consider the Pauli principle in the motion of the particles. Usually the Pauli principle is only dealt with in the collision term. In how far a so called "Pauli potential" can simulate the fermionic dynamics will be discussed in section 3.3.

3.2 Shell structure in FMD

It is not immediately obvious that FMD includes shell-model features like the nodal structure of single-particle orbits since the states are localized in coordinate and momentum space. One should however keep in mind that any unitary transformation among the occupied single-particle states leaves the antisymmetrized many-body state invariant. Therefore, after antisymmetrization, any set of single-particle states which is complete in the occupied phase space is as good as any other. This applies also to non-orthogonal states. To illustrate this we take four one-dimensional real gaussians with the same real width parameter a and zero mean momentum and displace them by $d = 0.75\sqrt{a}$ (see l.h.s. of fig. 3).

The one-body density, given in eq. (35), can be written in terms of orthonormal

states $|\psi_m\rangle$ as

$$\underset{\sim}{\rho}^{(1)} = \sum_{k,l=1}^{A} |q_k\rangle \, \mathcal{O}_{kl} \, \langle q_l| = \sum_{m=1}^{A} |\psi_m\rangle\langle\psi_m| \ , \tag{63}$$

where the orthonormal eigenstates of $\underset{\sim}{\rho}^{(1)}$ are given by

$$|\psi_m\rangle = \sum_{k=1}^{A} |q_k\rangle \, (\mathcal{O}^{\frac{1}{2}})_{km} \ . \tag{64}$$

They are displayed on the right hand side of fig. 3 and compared to harmonic oscillator eigenstates (dashed lines). One sees that the orthogonal basis consists of an s-, p- ,d- and an f-state, all very close to harmonic oscillator states. The difference between both sets can be made arbitrarily small by letting $d/\sqrt{a}$ approach zero. This equivalence of gaussians, which have almost identical mean values, and the harmonic oscillator shell-model states is realized in the ground state of ^{16}O shown in section 3.1.

A second example is illustrated in fig. 4, where we consider 100 equally spaced gaussians in one dimension [24]. Again all mean momenta are zero and the width a is real. In the upper part of fig. 4 the width $\sqrt{a}$ is 0.2 of the mean distance d so that the wave packets are well separated. Therefore the spatial density ρ_x and the momentum density ρ_k are not changed by antisymmetrization. In the lower part the width has been increased to $\sqrt{a} = d$. Without antisymmetrization (dash dotted line) the spatial density is uniform and the momentum distribution is that of a single packet. After antisymmetrization (full lines) one obtains the typical shell model oscillations in coordinate space and a Fermi distribution in momentum space. It is amazing to see how in

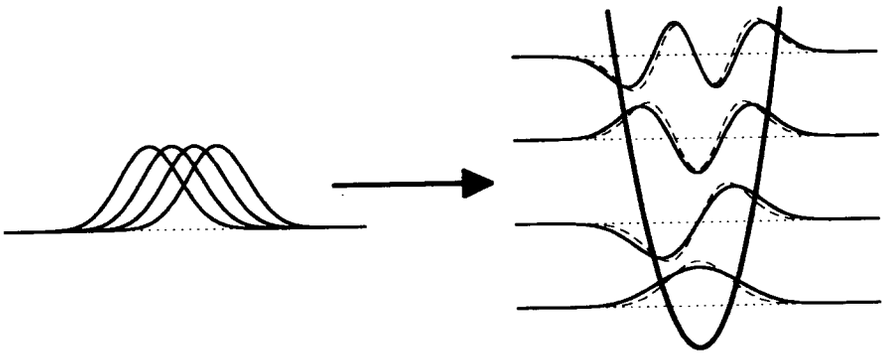

Fig. 3. Antisymmetrization of the four gaussians on the left hand side leads to harmonic oscillator states. Dashed lines are the exact eigenstates of the oscillator.

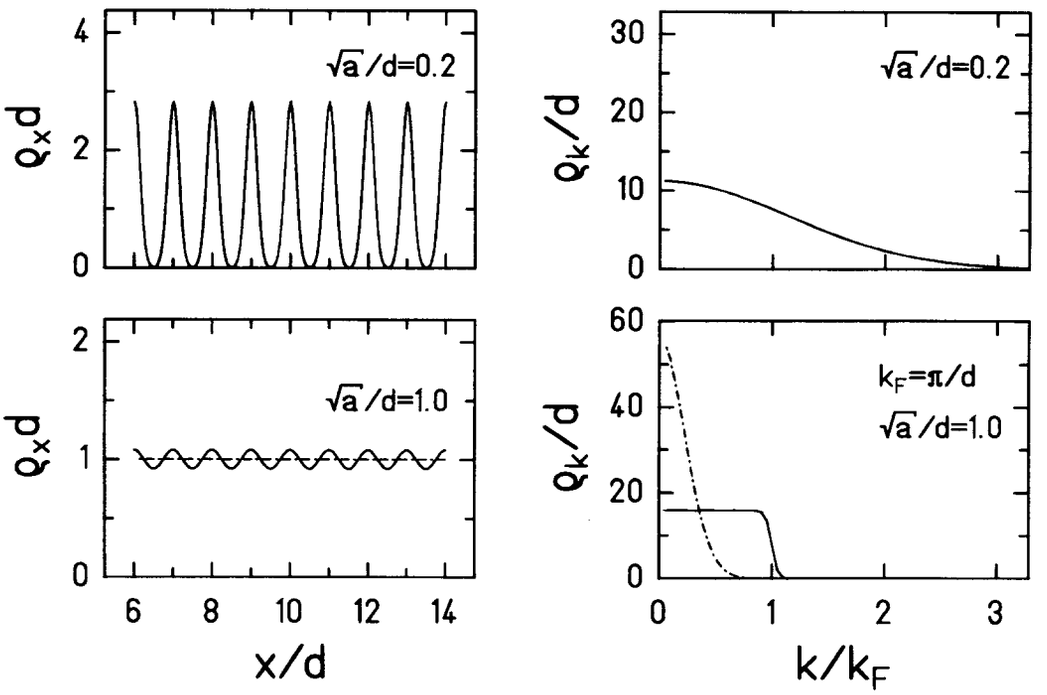

Fig. 4. Upper part: section of spatial density of hundred gaussians (not overlapping in coordinate space) and corresponding momentum distribution (same for all). Antisymmetrization does not change distributions. Lower part: same as above but for overlapping gaussians. Full line with antisymmetrization, dash-dotted line without. For details see text.

eq. (63) the superposition of gaussians by means of the inverse overlap matrices can create a fully occupied momentum state, see for example in fig. 4 the lower right momentum distribution at $k = 0.8k_F$, where the individual gaussians give practically zero probability to measure this momentum. We also calculated the eigenstates of the kinetic energy in the occupied space and got perfect sinusoidal waves.

These two examples illustrate nicely that even localized single-particle states with zero mean momentum build up FMD many-body trial states which describe the harmonic oscillator shell-model or even the Fermi motion of a gas of fermions in which plane waves are occupied up to the Fermi momentum.

If one wants to simulate this effect by a "Pauli potential", disregarding the momentum distribution in each wave packet, the resulting ground state momentum-distribution is unsatisfactory [12].

3.3 The effect of the Pauli principle on the trajectories

In this section we investigate the influence of the antisymmetrization on the trajectories [23,24]. In FMD it is not possible to simply switch on or off the Pauli principle because it is a genuine property of the trial state. The alternative to the antisymmetric state is a product state of distinguishable particles, as has been used for example by Konopka et al. [26]. There is, however, no direct comparison possible between FMD and a model which is based on a many-body product state composed of the same single-particles wave packets. The reason is that already the initial conditions, namely the ground states, cannot be chosen to be the same. The FMD ground state would not be stationary in the product ansatz model and vice versa the ground state of the product ansatz would be an excited state in FMD.

However, for nuclei which consist at most of two protons and two neutrons one may freeze the spins and iospins in opposite directions and then the antisymmetric state gives the same results as the product state. Therefore, we study the time evolution of two colliding Helium nuclei and compare the FMD results with those of the product state. As long as the Helium nuclei are separated, the time evolution with and without Pauli principle is the same. When two wave packets which belong to different ^{4}He, but have the same spin and isospin, begin to overlap the effect of the antisymmmetrization on the dynamics sets in. In fig. 5 the time-dependence of various quantities is displayed for a ^{4}He + ^{4}He central collision at 0.2 AMeV which leads to a long lived vibrating ^{8}Be. In the first row the decomposition of the total energy $\mathcal{H} = \langle \underset{\sim}{H} \rangle$ into kinetic energy $\langle \underset{\sim}{T} \rangle$ and potential $\langle \underset{\sim}{V} \rangle$ is shown as a function of time. The second row contains the longitudinal quadrupole moment, the square root of which can be regarded as a measure of the distance between the nuclei. The following three rows depict the parameters $r_x(t), p_x(t), a_R(t)$ and $a_I(t)$ of wave packet 1 (left hand nucleus) and 5 (right hand nucleus), which have the same spin and isospin. In contrast to the quadrupole moment the parameters are in general not measurable. The last row shows the overlap between $|\, q_1(t) \,\rangle$ and $|\, q_5(t) \,\rangle$. Due to the symmetries in this collision and in the interaction all the other parameters are either the same or have opposite sign.

The first column is the result of the FMD model. When the nuclei get close they first accelerate due to the attraction but then the wave packets are repelled whenever the overlap grows (peaks in last row). Alltogether the parameters of the system execute complicated nonlinear coupled oscillations. The second column has been obtained by calculating the same collision but with a product state as the trial state. The first prominent difference is that in this case the wave packets pass through each other from one side to other. The measurable quadrupol moment drops to zero which is not the case in FMD. Second, the oscillations are much faster and more violent, see the width parameters. The

reason is that the ^{8}Be nucleus is much more bound in a product state than in reality because the exchange terms which give a positive contribution to the energy are missing. Therefore the total energy of the fused system, which is the same in both cases, leads to little excitation in the FMD case but to a highly excited product state, see $\langle \underset{\sim}{V} \rangle$ in the first row. It is also interesting to note that the overlaps remain rather small. Whenever the packets overlap strongly in coordinate space they have large relative momenta and vice versa. This shows that the smallness of the overlaps in a calculation without antisymmetrization cannot be used as an argument in favour of neglecting the fermionic nature of the nucleons.

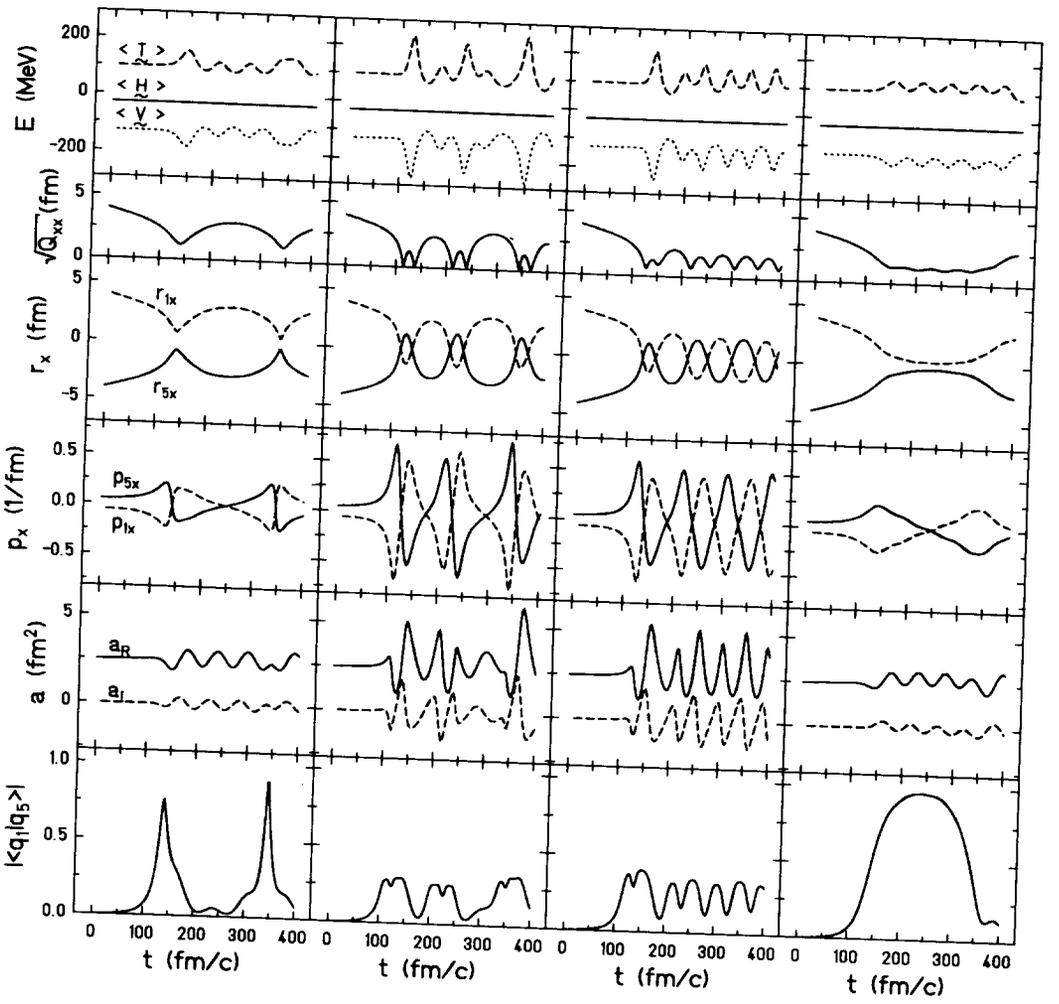

Fig. 5. Effect of Pauli principle on trajectories illustrated by various observables and parameters for a central ^{4}He + ^{4}He collision. From left to right: FMD; product many-body state (distinguishable particles); product many-body state but exchange terms in two-body interaction kept; forces $-\partial\mathcal{H}/\partial q_\mu$ calculated in antisymmetric fashion but classical $\mathcal{A}$-matrix. For details see text.

In the third column we put back one aspect of the Pauli principle, namely the exchange term in the two-body matrix elements. The product trial state is still kept but $\langle \underset{\sim}{V} \rangle$ is replaced by $\sum_{k,l} \langle q_k, q_l \,|\, \underset{\sim}{V} \,|\, q_k, q_l - q_l, q_k \rangle / \langle q_k, q_l \,|\, q_k, q_l - q_l, q_k \rangle$. This is a situation somewhat similar to the treatment of the mean field part in QMD where one uses the gaussian density packets of a product state together with a phenomenological interaction, which originates from the Skyrme-Hartree-Fock hamiltonian. In this picture the energy is regarded as a functional of the density and exchange effects are contained in the functional so that the expectation value of the energy is formally calculated in the Hartree approximation (product state). Again one sees much stronger oscillations and more excitation in the fused system.

In the fourth column we investigate the influence of the Pauli principle via the skew-symmetric $\mathcal{A}$ matrix. For that we calculate $\mathcal{H}$ and the forces $-\partial\mathcal{H}/\partial q_\nu$ in the fully antisymmentric fashion, but $\langle i\frac{d}{dt} \rangle$ and the resulting $\mathcal{A}$-matrix is calculated with the product state. In that case the $\mathcal{A}$-matrix assumes the classical canonical form (12) for the following pairs of canonical variables: $(\boldsymbol{p}_k\,,\, \boldsymbol{r}_k)$ for positions, $(\alpha_k := -3/(4a_{Rk})\,,\, a_{Ik})$ for widths, and $(\phi_k\,,\, s_k := \frac{1}{2}\cos\chi_k)$ for spins. The equations of motion for $\boldsymbol{p}_k(t)$ and $\boldsymbol{r}_k(t)$ and also for the other canonical variables have now the classical form

$$\begin{aligned}
\frac{d}{dt}\boldsymbol{p}_k(t) &= -\frac{\partial\mathcal{H}}{\partial \boldsymbol{r}_k} \quad \text{and} \quad \frac{d}{dt}\boldsymbol{r}_k(t) = \frac{\partial\mathcal{H}}{\partial \boldsymbol{p}_k}\,, \\
\frac{d}{dt}a_{Ik}(t) &= -\frac{\partial\mathcal{H}}{\partial \alpha_k} \quad \text{and} \quad \frac{d}{dt}\alpha_k(t) = \frac{\partial\mathcal{H}}{\partial a_{Ik}}\,, \\
\frac{d}{dt}s_k(t) &= -\frac{\partial\mathcal{H}}{\partial \phi_k} \quad \text{and} \quad \frac{d}{dt}\phi_k(t) = \frac{\partial\mathcal{H}}{\partial s_k}\,,
\end{aligned} \tag{65}$$

but we are dealing with the wrong canonical variables.

From the numerical results in column 4 we see that the excitation of the system is similar to FMD, but the time evolution is completely different. In FMD large overlaps cause strong deviations of the fermionic $\mathcal{A}$ from the classical one and the result is a repulsion of the wave packets. This is not seen with the classical $\mathcal{A}$ where the overlap becomes large and stays large.

From this results it seems doubtful to incorporate the effects of the Pauli principle by means of adding a Pauli-potential, $\mathcal{H} \rightarrow \mathcal{H} + \mathcal{V}_{Pauli}$, while keeping classical Hamilton's equation of motion for $\boldsymbol{p}_k$ and $\boldsymbol{r}_k$ and regarding them as the canonical variables [2,11,12].

To summarize, the Pauli principle enters the equation of motion for the parameters at two places. First, the energy (Hamilton function $\mathcal{H}(Q)$) is modified and gets additional momentum dependences. In addition it is not a two-body

interaction any more, in the sense

$$\mathcal{H}(Q) = \mathcal{H}(q_1, q_2, \cdots, q_A) \neq \sum_k T^{(1)}(q_k) + \sum_{k<l} V^{(2)}(q_k, q_l) \ , \tag{66}$$

because due to the inverse overlap matrices $\mathcal{O}_{kl}$ the hamiltonian $\mathcal{H}(Q)$ contains A-body correlations between the parameters, c.f. eqs. (37) and (41). Second, the nonclassical $\mathcal{A}$ matrix contains also A-body correlations in parameter space, because $\mathcal{A}_{\mu\nu} \neq 0$ for ν and μ belonging to different wave packets (particles).

It is important to realize that the Pauli principle influences the trajectories through $\mathcal{A}(Q)$ like virtual forces which appear when one is using curved spaces. $\mathcal{A}(Q)$ thus plays the role of a metric. One may argue that one is allowed to choose a phenomenological $\mathcal{H}(Q)$, since the effective nucleon-nucleon interaction is not known anyhow, but one has no freedom in choosing $\mathcal{A}(Q)$ because this is a purely geometric quantity which depends only on the way the trial state is parametrized and $\mathcal{A}(Q)$ does not depend on the interaction.

For fermions without interactions ($\underset{\sim}{H} = \underset{\sim}{T}$) the solution of the FMD equations are (c.f. eq. (52))

$$\dot{\boldsymbol{r}}_k = \frac{\boldsymbol{p}_k}{m} \ , \ \dot{\boldsymbol{p}}_k = 0 \ , \ \dot{a}_{Rk} = 0 \ , \ \dot{a}_{Ik} = \frac{1}{m_N} \ , \ \dot{\chi}_k = 0 \ , \ \dot{\phi}_k = 0 \ , \tag{67}$$

and the resulting many-body state $|\,Q(t)\,\rangle$ is the exact solution of the many-body Schrödinger equation.

In the case of free motion there is no influence of the Pauli principle on the *parameters*, a product state results in the same solution (67) for the parameters. The centroids of the packets move on straight lines while they are spreading according to the imaginary part of the width: $a_{Ik}(t) = t/m_N + a_{Ik}(t_0)$. Nevertheless, the Pauli principle is present in the antisymmetric many-body state $|\,Q(t)\,\rangle$. If one asks for the probability of finding two identical fermions at the same point in phase space the two-body density $\rho^{(2)}$ belonging to $|\,Q(t)\,\rangle$ (eq. (38)) will give zero probability, even if the wave packets are strongly overlapping. The product state would of course not give this answer.

If one freezes the width parameter as a dynamical variable virtual forces appear through $\mathcal{A}(Q)$ and there is scattering even without any interaction [10]. For this and other reasons, mentioned later, it is advisable to include the complex widths $a_k(t)$ as dynamical variables in the trial state.

3.4 $^6Li + {}^4He$ collisions at $E_{lab} = 4.7$ A MeV

The density contour plots in fig. 6 display the collision of a (deformed) ^{6}Li nucleus with a (spherical) ^{4}He at $E_{LAB} = 4.7$ AMeV and an impact parameter $b = 1.4$ fm. The crosses indicate again the centroids of the wave packets. The two nuclei touch, merge and the α-particle orbits around the ^{6}Li. During the reaction the ^{6}Li gets highly excited and at $t = 150$ fm/c its density has dropped to about half of the ground state density. The expansion is followed by contraction of four wave packets to form an α-particle and the emission of a proton and a neutron. The emitted particles occupy packets which have spread dramatically in coordinate space and correspondingly shrunk in momentum space. Only the outer most contour line, which is at 0.005 of the initial maximum density, and the cross reveal their presence (see $t = 275$ through $t = 325$ fm/c). Finally after the collision one observes two α-particles with a scattering angle of about 90 degrees in the lab-frame, one more, the other one less excited, and two free nucleons with the same mean position, therefore only one cross is seen.

In fig. 7 the initial state differs from the one shown in fig. 6 by rotating the ^{6}Li nucleus by 90 degrees. The impact parameter and the energy remain unchanged. In this reaction the final state consists again of two α-particles and two promptly emitted nucleons but the reaction products are created in a completely different way. Two wave packets of the initial α-particle pull along two wave packets of the ^{6}Li to form the final α-particle seen in the lower left corner of the last frame at $t = 475$ fm/c. The remaining two packets of the initial α go together with the two packets which were originally in the centre of the ^{6}Li and build the final α on the right hand side. During this exchange process the right most two nucleons of the ^{6}Li get lost and form during $t = 300-400$ fm/c a highly excited deuteron which decays subsequently into a free proton and neutron. It should be mentioned that the V2 interaction together with the gaussian packets gives only a very poor description of the deuteron.

An important result of this application of FMD to colliding nuclei is that the final channels are characterized by large fluctuations qualitatively in accordance with experimental findings. In the following section we discuss the quantal interpretation of the different initial orientations in connection with many-body correlations and the formation of fragments.

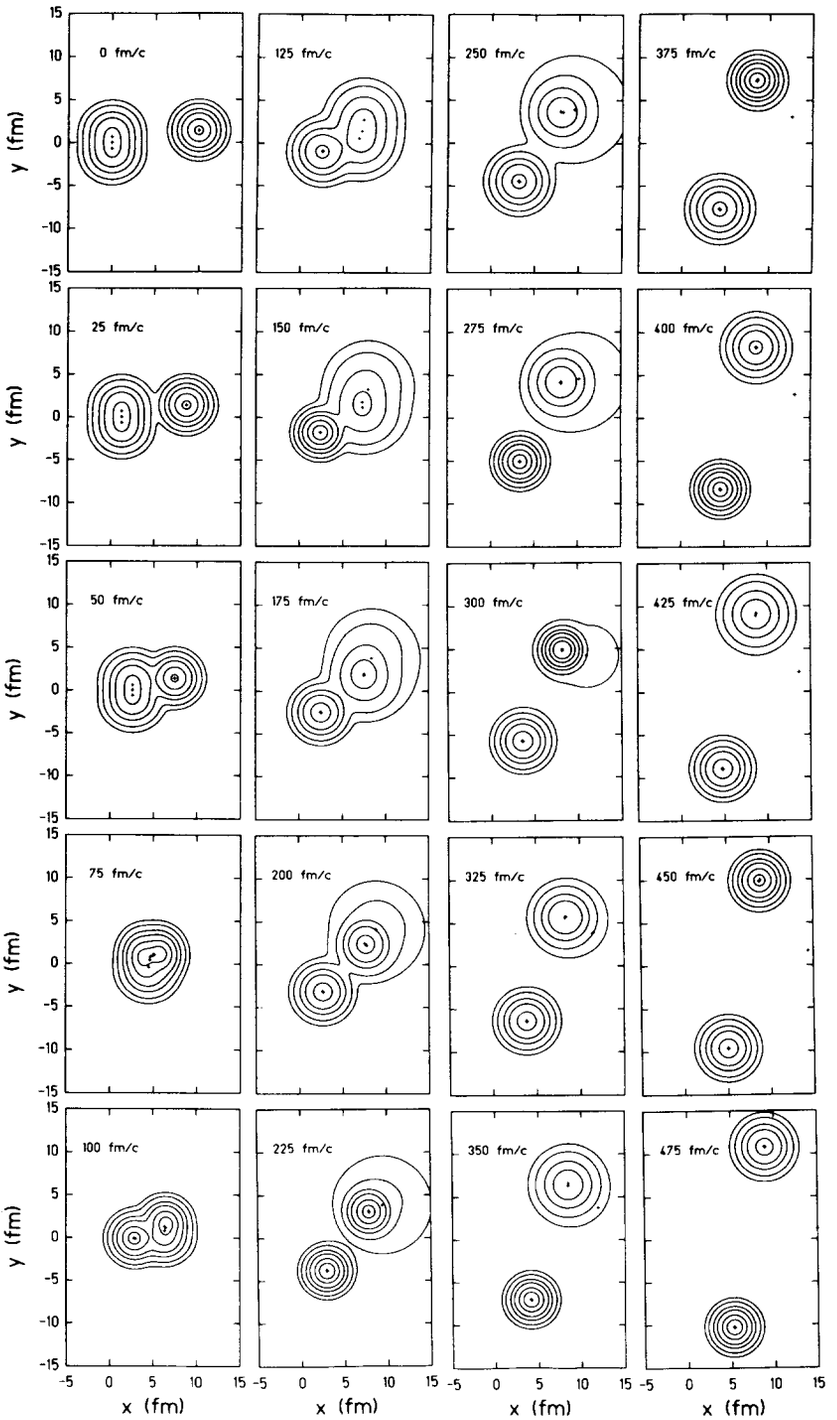

Fig. 6. Contour plot of spatial density at $z = 0$ for ^{4}He + ^{6}Li at $E_{LAB} = 4.7$ AMeV and impact parameter $b = 1.4$ fm. Countour lines are at 0.005, 0.02, 0.08, 0.2, 0.5, 0.9 of maximum density at $t = 0$.

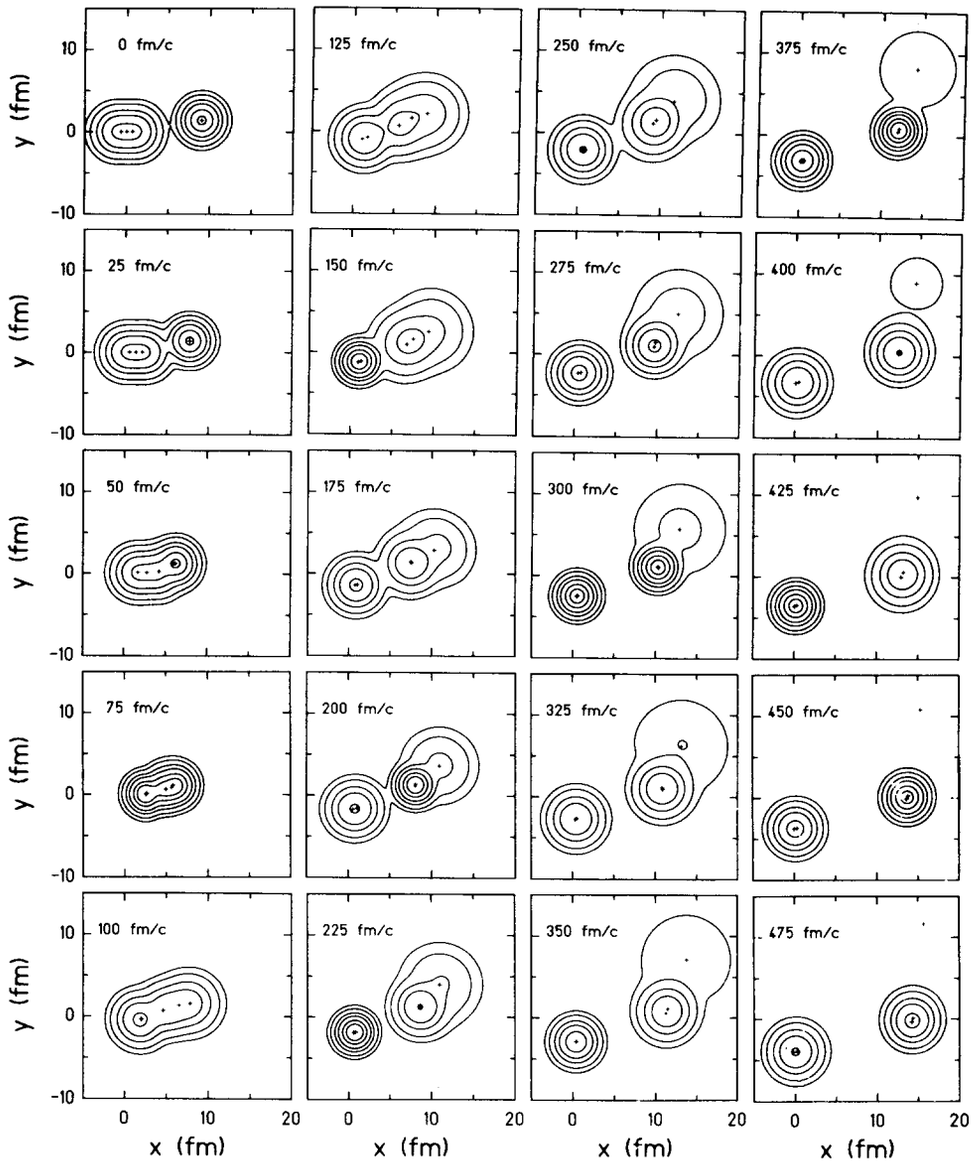

Fig. 7. Same as fig. 6 but initial orientation of ^{6}Li along beam axis.

3.5 *Definition of the ensemble and fluctations therein*

Although the hamiltonian is rotationally invariant the ground states are in general not eigenstates of the total spin operator $\underset{\sim}{J}^2$ and $\underset{\sim}{J}_z$ but are deformed in coordinate and momentum space. The breaking of the rotational symmetry is of course due to the restriction of the many-body trial state to a single Slater determinant. The deformations reflect many-body correlations between the nucleons in the sense that within the manifold a trial state with a special order in the relative positions and momenta of the nucleons is lower in energy than a spherically symmetric configuration. For example in ^{12}C an arrangement in which groups of four wave packets form three α-clusters in a triangle is energetically preferred. Or, if one takes the ^{8}Be ground state (see fig. 2) the correlation between the two protons with spin up is such that if one proton is in the left hand α-cluster the other one is in the right hand cluster. This two-body correlation does not exist in a spherical Slater determinant which contains only correlations due to the Pauli principle. Therefore, one may not argue that by definition a single Slater determinant does not contain many-body correlations. In some sense the variational principle tries to make up for the deficiencies in the trial state by breaking the symmetry.

The FMD ground states introduced in section 3.1 have to be treated like intrinsically deformed Hartree Fock states. Ground states with good spin quantum numbers are obtained with help of rotation matrices by projecting the FMD ground states [27]. A $J^\pi = 0^+$ state is constructed by

$$|\, GS; J^\pi = 0^+ \,\rangle = \frac{1}{\sqrt{N}} \int d^3\Omega \; \mathcal{D}^0_{00}(\Omega) \;\; |\, Q_{GS}; \Omega \,\rangle \;, \tag{68}$$

where

$$|\, Q_{GS}; \Omega \,\rangle := \exp\{-i\Omega \underset{\sim}{J}\} \, |\, Q_{GS} \,\rangle \tag{69}$$

is the deformed FMD ground state rotated with the three Euler angles Ω. If the ground state is not a $J^\pi = 0^+$ state the rotation matrix $\mathcal{D}^0_{00}(\Omega) = 1$ has to be replaced by the appropriate $\mathcal{D}^J_{M0}(\Omega)$.

The initial state of a heavy-ion collision is therefore a coherent superposition of all orientations of the two nuclei:

$$|\, \Psi(t=0) \,\rangle = \frac{1}{\sqrt{N_1 N_2}} \int d^3\Omega_1 d^3\Omega_2 \;\; |\, Q(t=0); \Omega_1, \Omega_2 \,\rangle \;, \tag{70}$$

where

$$|\, Q(t=0); \mathbf{\Omega}_1, \mathbf{\Omega}_2 \,\rangle = \underset{\sim}{A} \left(|\, Q_{GS1}; \mathbf{\Omega}_1 \,\rangle \otimes |\, Q_{GS2}; \mathbf{\Omega}_2 \,\rangle \right) \tag{71}$$

denotes the antisymmetrized product of the two boosted ground states with orientations $\mathbf{\Omega}_1$ and $\mathbf{\Omega}_2$ placed at a distance from each other and N_1, N_2 are the respective norms.

The exact time evolution of this state is given by the relation

$$|\, \Psi(t) \,\rangle_{exact} = \frac{1}{\sqrt{N_1 N_2}} \int d^3\Omega_1 d^3\Omega_2 \; \exp\{-i \underset{\sim}{H}\, t\} \, |\, Q(t=0); \mathbf{\Omega}_1, \mathbf{\Omega}_2 \,\rangle \tag{72}$$

which can be interpreted as follows. With a certain amplitude (here $1/\sqrt{N_1 N_2}$) the two nuclei collide while they are in their intrinsic states $|\, Q_{GS1}; \mathbf{\Omega}_1 \,\rangle$ and $|\, Q_{GS2}; \mathbf{\Omega}_2 \,\rangle$, respectively. Because of the linearity of the time propagator at any time t throughout the collision the exact many-body state is always the average over all initial orientations $\mathbf{\Omega}_1$ and $\mathbf{\Omega}_2$ weighted with the initial time-independent amplitudes. The same holds of course for the finally measured state.

In the spirit of a semi-classical approximation the exact solution for a given pair of orientations $\mathbf{\Omega}_1$ and $\mathbf{\Omega}_2$ is replaced by the FMD solution

$$\exp\{-i \underset{\sim}{H}\, t\} \, |\, Q(t=0); \mathbf{\Omega}_1, \mathbf{\Omega}_2 \,\rangle \rightarrow |\, Q(t); \mathbf{\Omega}_1, \mathbf{\Omega}_2 \,\rangle \;, \tag{73}$$

where $|\, Q(t); \mathbf{\Omega}_1, \mathbf{\Omega}_2 \,\rangle$ is evolved in time according to the FMD equations of motion. The semiclassical state $|\, \Psi(t) \,\rangle_{FMD}$ at time t is herewith a coherent superposition of FMD states at time t which had the initial orientations $\mathbf{\Omega}_1$ and $\mathbf{\Omega}_2$.

$$|\, \Psi(t) \,\rangle_{exact} \rightarrow |\, \Psi(t) \,\rangle_{FMD} = \frac{1}{\sqrt{N_1 N_2}} \int d^3\Omega_1 d^3\Omega_2 \; |\, Q(t); \mathbf{\Omega}_1, \mathbf{\Omega}_2 \,\rangle \;. \tag{74}$$

In fig. 8 a few initial orientations are selected and evolved in time with the FMD equations. While the superposition of the left hand column represents the initial state with the spherical ground states, the same superposition of the right hand column is according to eq. (74) the final semiclassical many-body state. Please note that one nucleus is ^{4}He which is already spherical so that only the $\mathbf{\Omega}_1$ of the deformed ^{6}Li can be varied.

Figure 8 also shows that the final individual FMD channels have practically no overlap anymore, i.e.

$$\langle\, Q(t \rightarrow \infty); \mathbf{\Omega}_1, \mathbf{\Omega}_2 \,|\, Q(t \rightarrow \infty); \mathbf{\Omega}'_1, \mathbf{\Omega}'_2 \,\rangle \propto \; \delta_{\Omega_1 \Omega'_1} \; \delta_{\Omega_2 \Omega'_2} \;. \tag{75}$$

This implies that for the expectation value of an arbitrary operator $\underset{\sim}{B}$ the coherent summation in eq. (74) turns into an incoherent average over the weighted initial orientations

$$\left\langle\left\langle \underset{\sim}{B} \right\rangle\right\rangle (t \to \infty) \approx \tag{76}$$
$$\left(\frac{1}{8\pi^2}\right)^2 \int d^3\Omega_1 d^3\Omega_2 \langle Q(t \to \infty); \mathbf{\Omega}_1, \mathbf{\Omega}_2 \,|\, \underset{\sim}{B} \,|\, Q(t \to \infty); \mathbf{\Omega}_1, \mathbf{\Omega}_2 \rangle \ .$$

Thus, $|\, Q(t); \mathbf{\Omega}_1, \mathbf{\Omega}_2 \,\rangle$ can be regarded as a member of an ensemble.

This is different from classical molecular dynamics or QMD where often random initial positions and random initial momenta of the particles constitute the ensemble. Since FMD has stationary ground states with the parameters

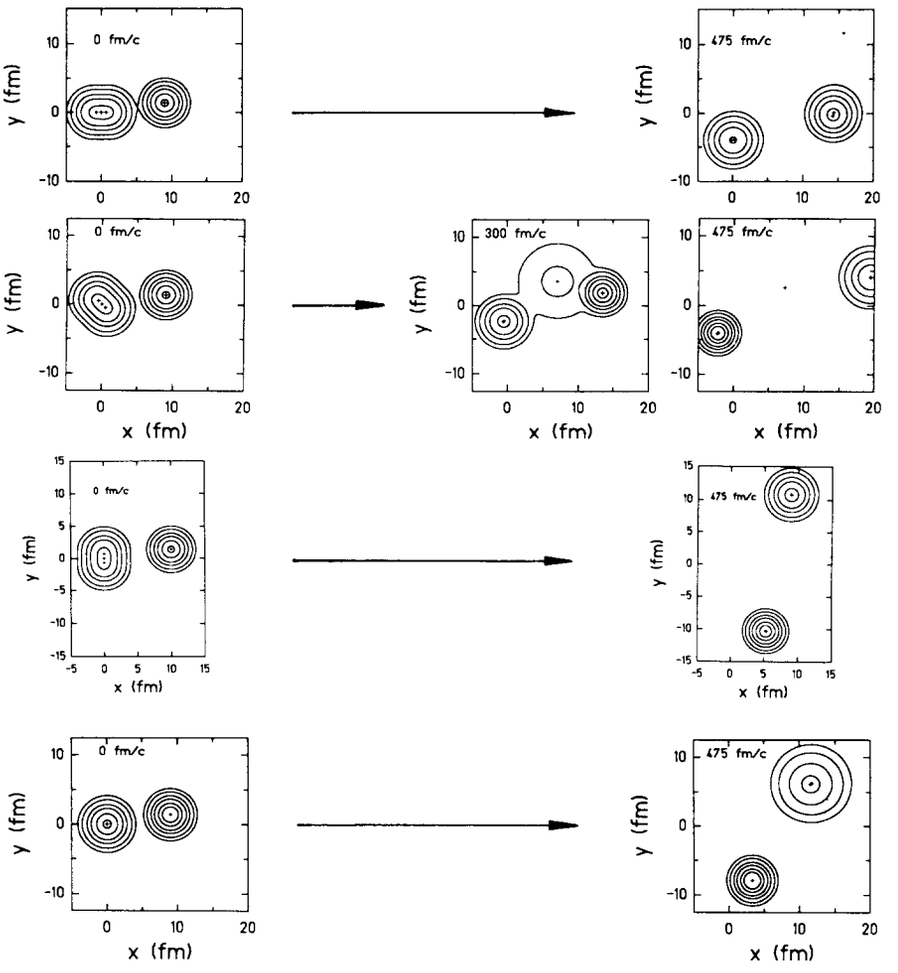

Fig. 8. Initial ensemble of different orientations of the intrinsic deformed ground states and final ensemble with large fluctuations. All collisions are ^{4}He + ^{6}Li at E_{LAB} = 4.7 AMeV and b = 1.4 fm.

given by the requirement of minimal total energy, the relative positions and momenta between the wave packets cannot be chosen at random. The ensemble in FMD consists of all orientations of the two deformed initial ground states, in accordance with the quantal picture discussed above.

Actually, the ensemble consists also of the different possibilities to choose an impact parameter. As in all other models for inelastic heavy-ion collisions we have tacitly supposed that the assumption (76) of incoherence in the final state applies also to the initial coherent superposition of impact parameters or angular momenta which one needs to set up an incoming plane wave in the relative motion of the centers of masses. The averaging over the initial orientations has to be understood in the same way as the averaging over the initial positions of the nuclei.

All collisions shown in fig. 8 are for the same impact parameter $b = 1.4$ fm and the same beam energy $E_{LAB} = 4.7$ AMeV but differ in the initial orientation $\mathbf{\Omega}_1$ of the ^{6}Li. The first row is the initial and final state of fig. 7 where a proton and a neutron are promptly emitted from the outer edge of the ^{6}Li. In the second row ^{6}Li is rotated by 45^0 which leads again to two excited α-particles but with the proton and neutron emitted from the neck. The cross indicates that their centroids are almost at rest but nevertheless they fly in all directions because the wave packets are spreading. The third row is taken from fig. 6 and discussed there. For the initial orientation displayed in the last row, where the orientation is out of the reaction plane, ^{6}Li survives as a highly excited nucleus without loosing particles before $t = 475$ fm/c.

This example and many others for heavier systems [24] show that FMD is capable of producing large fluctuations in the final channels. They originate from quantal fluctuations in the orientation of the intrinsically deformed initial ground state.

Each row in fig. 8 shows the expectation value

$$\left\langle \underset{\sim}{\varrho}(\boldsymbol{x}) \right\rangle = \langle\, Q(t); \mathbf{\Omega}_1, \mathbf{\Omega}_2 \,|\, \underset{\sim}{\varrho}(\boldsymbol{x}) \,|\, Q(t); \mathbf{\Omega}_1, \mathbf{\Omega}_2 \,\rangle$$

of the spatial density. If one superimposes the different rows of the FMD results one obtains the ensemble averaged one-body density $\left\langle\left\langle \underset{\sim}{\varrho}(\boldsymbol{x}) \right\rangle\right\rangle$ according to eq. (76) ($\underset{\sim}{B}$ replaced by $\underset{\sim}{\varrho}(\boldsymbol{x})$). It is obvious that for fragmentation reactions mean-field theories like VUU or BUU [28–32] which are based on the ensemble averaged one-body phase-space distribution can make sense only in the initial stage of the collision up to the time when the system expands and decays into clusters. The final $\left\langle\left\langle \underset{\sim}{\varrho}(\boldsymbol{x}) \right\rangle\right\rangle$ is a highly diluted density smeared over a large area without any resemblance of the outcoming clusters. In the expansion phase of a fragmentation reaction many-body correlations which are not contained in an ensemble averaged one-body density govern the dynamics.

It is evident that the amount of fluctuation will depend on the size of the deformation in the initial state. This effect has already been seen experimentally in low energy fusion reactions where the orientations of the intrinsic deformation leads to fluctuations of the fusion barrier [33,34].

3.6 The dynamical complex width parameter

In fig. 9 the coordinate space density of a collision between ^{7}Li and ^{15}N is displayed for two energies, E_{LAB} = 6.8 AMeV (upper part) and E_{LAB} = 28.7 AMeV (lower part). For identical initial impact parameter (b = 0.5 fm) and orientations of the two nuclei we compare the time evolution using the complete set of parameters with the one where all complex width parameters

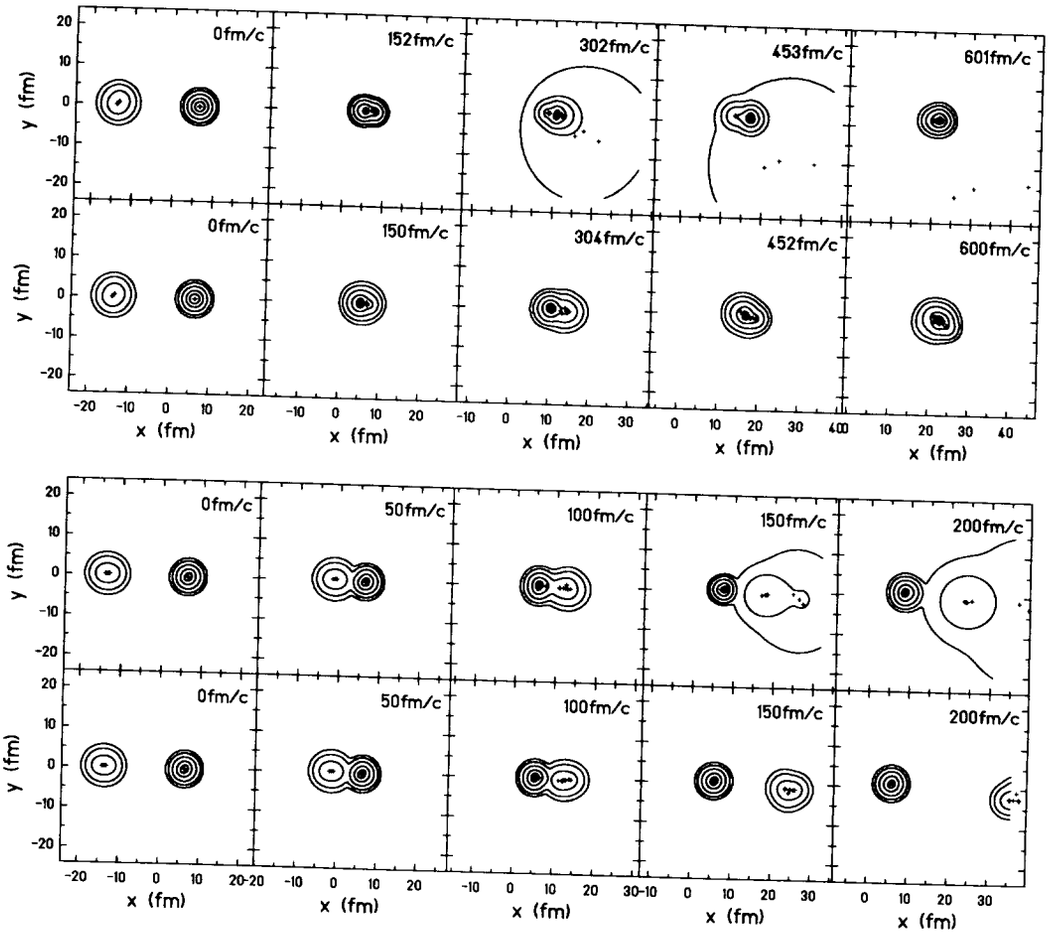

Fig. 9. Comparison with frozen widths parameters. First and third row with $a_k(t)$ time-dependent; second and fourth row a_k = initial ground state values. Reaction ^{7}Li + ^{15}N at b = 0.5 fm. Upper frame for E_{LAB} = 6.8 AMeV; lower frame for E_{LAB} = 28.7 AMeV.

a_k have been kept fixed at their initial ground state values.

At E_{LAB} = 6.8 AMeV the ^{7}Li merges around t = 152 fm/c with the ^{15}N and shrinks in size due to the attraction with the Nitrogen nucleons. But around 302 fm/c it becomes obvious that the three weakly bound nucleons in the p-shell are wiped off. The lowest density contour line, which extends far out, indicates that the three wave packets, with their centroids (crosses) already outside the fused ^{19}F nucleus, are spreading fast while moving away. One should however keep in mind that the V2 interaction gives only a very poor description of the ^{7}Li ground state. As can be seen from table 2 the binding energy is too little and the radius is too big. But even though the ground state is not realistic the reaction shows that FMD is sensitve to the structure of the initial state. The loosely bound proton and two neutrons are behaving different than the s-shell nucleons which form a ^{4}He core.

The second row in the upper frame shows the same reaction but all width parameters a_k are removed from the set of dynamical variables. Here the system fuses without emission of particles. The reason is that a fixed width implies a zero-point energy in each packet of about $\varepsilon_{kin} = 3/(4m_N a_R) \approx$ 10 MeV. Inside the nucleus this energy is part of the kinetic energy in the Fermi motion. Outside the nucleus the zero-point energy of an emitted particle is determined by the amount of its localization at the end of the emission process. If the width is kept fixed the nucleon carries besides its mean energy always the additional 10 MeV.

Compared to that a wave packet with a dynamical width escapes from a nucleus by first spreading, i.e. a_{Rk} and a_{Ik} become very large [24], which has two effects: first, the large spatial extend leaves little overlap with the other packets and the negative potential energy tends to zero, second, the positive zero-point energy also becomes small so that the sum of both need not change too much during the emission. Classically spoken, a particle leaving the nucleus has to climb up the surface potential-wall loosing almost all of its kinetic energy before escaping. FMD gives values of about 2 MeV for the kinetic energy of evaporated particles in accord with experimental findings. The emission of a wave packet with fixed width is very unprobable because it carries away at least its zero-point energy of 10 MeV leaving the residual nucleus at lower excitation energy where the level density is much smaller.

These problems do not arise in QMD as the momentum distribution of the packets is nowhere taken into account. In AMD a subtraction of spurious zero-point oscillations is performed [9] which also takes care of the localization energy in the center-of-mass motion of the fragments.

The lower frame in fig. 9 shows the same collision but for E_{LAB} = 28.7 AMeV. Here the ^{7}Li is completely desintegrated. At t = 150 fm/c one sees that the

three loosely bound nucleons in ^{7}Li are distached from the remaining ^{4}He-core which however is so highly excited that it also finally decays. In the case of fixed widths the ^{7}Li remains intact after the collision and does not show any sign of decay up to 200 fm/c. The reason is the same as discussed above.

The two examples show that the complex width parameter is an important degree of freedom and should be included as a dynamical variable in the trial state.

4 Outlook

The variety of phenomena seen in the reactions displayed in this paper and elsewhere [24,25] promoted the idea to develop approximations to be able to calculate enough events for a quantitative comparison with measured data. Since most of the computer time is consumed in working out for each time step A^4 (A = particle number) two-body matrix elements and there derivatives which are multiplied with two inverse overlap matrices in a 3- and 4-fold summation (c.f. eq. (50)), we first try to approximate the potential energy. Without antisymmetrization the effort is propotional only to A^2. But one should resist the temptation to neglect the antisymmetrization as it is essential for having the correct Fermi dynamics and shell structure of the initial nuclei and the produced fragments, as shown in section 3.1 3.2, and 3.3. Approximations retaining the properties of antisymmetrization are being tested know and they allow to do calculations up to about $A = 40$.

Besides the more technical questions how to speed up the computation there is the quest for a successful effective interaction which not only gives correct binding energies and radii for all nuclei from ^{2}H to ^{238}U but also includes the repulsive hard core. In nuclear matter the short range repulsion is essential for correct saturation properties and in collisions of nuclei it is the origin of hard collisions with large momentum transfer populating unoccupied parts of the phase space. The saturation aspect is usually taken care of by a density dependent two-body interaction or a three-body contact interaction as in Skyrme-Hartree-Fock, where the many-body wave function is also a Slater determinant. For ground states the effective interactions for simple shell-model like states are very successful but in the dynamical situation of a heavy ion reaction individual collisions between the particles occur which cannot be treated in an averaged way by a density dependence. In most models (like BUU, QMD, AMD) one therefore introduces these collisions explicitly by a random force which is changing the momenta of the nucleons from time to time in a discontinuous way according to recipes based on a Boltzmann collision term. Besides the conceptual problem how to divide the interaction into a mean-field part and a collision term, the disadvantage of a random force is that it may

A Appendix

It turns out that the all expressions can be written in a convenient way using the parametrization

$$q_k = \{ \boldsymbol{b}_k, \boldsymbol{b}_k^*, a_k, a_k^*, \phi_k, \chi_k \} , \tag{A.1}$$

where the complex parameters $\boldsymbol{b}_k$ and a_k and their complex conjugate $\boldsymbol{b}_k^*$ and a_k^* are taken as independent variables. $\boldsymbol{b}_k$ and a_k consist of real and imaginary parts, denoted by the the subscript R and I, respectively. The relation with the other parameters are

$$\boldsymbol{b}_k = \boldsymbol{b}_{Rk} + i\,\boldsymbol{b}_{Ik} = (\boldsymbol{r}_k - a_{Ik}\,\boldsymbol{p}_k) + i\,(a_{Rk}\,\boldsymbol{p}_k) \tag{A.2}$$

$$a_k = a_{Rk} + i\,a_{Ik} . \tag{A.3}$$

The single-particle states defined in eq. (23) written in terms of the parameters (A.1) assume the form

$$\langle \boldsymbol{x} \,|\, q_k(t) \rangle = \exp\left(- \frac{(\boldsymbol{x} - \boldsymbol{b}_k(t))^2}{2\,a_k(t)} \right) |\, \chi_k(t), \phi_k(t) \rangle \otimes |\, m_t(k) \rangle , \tag{A.4}$$

which we shall use in the following.

A.1 One-body matrix elements and their derivatives

The derivative of the expectation value of an one-body operator with respect to one of the parameters can be expressed conveniently in terms of the derivative of the one-body density (see eq. (35))

$$\underset{\sim}{\rho}^{(1)} = \sum_{k,l=1}^{A} |\, q_l \rangle\, \mathcal{O}_{lk}\, \langle\, q_k \,| \tag{A.5}$$

as

$$\begin{aligned} \frac{\partial \underset{\sim}{\rho}^{(1)}}{\partial q_\mu} = & \sum_{l=1}^{A} |\, \frac{\partial}{\partial q_\mu} q_m \rangle\, \mathcal{O}_{ml}\, \langle\, q_l \,| + \sum_{k=1}^{A} |\, q_k \rangle\, \mathcal{O}_{km}\, \langle\, \frac{\partial}{\partial q_\mu} q_m \,| \\ & - \sum_{k,l=1}^{A} |\, q_k \rangle \left[\sum_{n=1}^{A} \mathcal{O}_{km} \langle\, \frac{\partial}{\partial q_\mu} q_m \,|\, q_n \rangle \mathcal{O}_{nl} + \mathcal{O}_{kn} \langle\, q_n \,|\, \frac{\partial}{\partial q_\mu} q_m \rangle \mathcal{O}_{ml} \right] \langle\, q_l \,| \end{aligned}$$

destroy delicate many-body correlations important to describe the formation of fragments.

We are not following the same route but rather preserve the spirit of the FMD model: the choice of the parametrized antisymmetric trial state determines which physical phenomena are included while the equations of motion for the parameters follow from the variational principle. Therefore, we are incorporating now short range repulsive correlations into the FMD trial state by means of a Jastrow ansatz [35]. In this way one allows for hard collisions more violent than those seen in this paper. A division into mean-field and collisions is avoided and the time evolution of each event is still deterministic. Unfortunately, the lagrangian cannot be calculated analytically anymore and cunning approximations are needed.

First results indicate that the ground states up to ^{40}Ca can be described well without overbinding and in heavy-ion reactions rapid variations of the many-body trial state occur, reflecting the collisions between the wave packets.

$$= 2\left(\frac{1}{4} + m_t(k)\, m_t(l)\right) \;, m_t = \begin{cases} \frac{1}{2} : proton \\ -\frac{1}{2} : neutron \end{cases} \tag{A.12}$$

The derivatives of the spin overlaps (A.11) are given by

$$\frac{\partial}{\partial \phi_k} \langle \chi_k, \phi_k \,|\, \chi_l, \phi_l \rangle = -i \sin\frac{\chi_k}{2} \sin\frac{\chi_l}{2} e^{-i(\phi_k - \phi_l)} \tag{A.13}$$

$$\frac{\partial}{\partial \chi_k} \langle \chi_k, \phi_k \,|\, \chi_l, \phi_l \rangle = \tfrac{1}{2}\left(-\sin\frac{\chi_k}{2}\cos\frac{\chi_l}{2} + \cos\frac{\chi_k}{2}\sin\frac{\chi_l}{2} e^{-i(\phi_k - \phi_l)}\right) . \tag{A.14}$$

The matrix elements of the Pauli spin matrices and their derivatives are

$$\langle \chi_k, \phi_k \,|\, \underset{\sim}{\sigma} \,|\, \chi_l, \phi_l \rangle = \begin{pmatrix} \cos\frac{\chi_k}{2}\sin\frac{\chi_l}{2} e^{i\phi_l} + & \sin\frac{\chi_k}{2}\cos\frac{\chi_l}{2} e^{-i\phi_k} \\ -i\cos\frac{\chi_k}{2}\sin\frac{\chi_l}{2} e^{i\phi_l} + & i\sin\frac{\chi_k}{2}\cos\frac{\chi_l}{2} e^{-i\phi_k} \\ \cos\frac{\chi_k}{2}\cos\frac{\chi_l}{2} - & \sin\frac{\chi_k}{2}\sin\frac{\chi_l}{2} e^{-i(\phi_k - \phi_l)} \end{pmatrix} \tag{A.15}$$

$$\frac{\partial}{\partial \phi_k} \langle \chi_k, \phi_k \,|\, \underset{\sim}{\sigma} \,|\, \chi_l, \phi_l \rangle = \begin{pmatrix} -i\sin\frac{\chi_k}{2}\cos\frac{\chi_l}{2} e^{-i\phi_k} \\ \sin\frac{\chi_k}{2}\cos\frac{\chi_l}{2} e^{-i\phi_k} \\ i\sin\frac{\chi_k}{2}\sin\frac{\chi_l}{2} e^{-i(\phi_k - \phi_l)} \end{pmatrix} , \tag{A.16}$$

$$\frac{\partial}{\partial \chi_k} \langle \chi_k, \phi_k \,|\, \underset{\sim}{\sigma} \,|\, \chi_l, \phi_l \rangle = \tfrac{1}{2} \begin{pmatrix} -\sin\frac{\chi_k}{2}\sin\frac{\chi_l}{2} e^{i\phi_l} + \cos\frac{\chi_k}{2}\cos\frac{\chi_l}{2} e^{-i\phi_k} \\ i\sin\frac{\chi_k}{2}\sin\frac{\chi_l}{2} e^{i\phi_l} + i\cos\frac{\chi_k}{2}\cos\frac{\chi_l}{2} e^{-i\phi_k} \\ -\sin\frac{\chi_k}{2}\cos\frac{\chi_l}{2} - \cos\frac{\chi_k}{2}\sin\frac{\chi_l}{2} e^{-i(\phi_k - \phi_l)} \end{pmatrix} . \tag{A.17}$$

The parameter are all time-dependent and b_k and a_k are complex. For the time derivative of the overlap matrix

$$\begin{aligned} \langle q_k \,|\, \frac{d}{dt} q_l \rangle = \dot{\boldsymbol{b}}_l \langle q_k \,|\, \frac{\partial}{\partial \boldsymbol{b}_l} q_l \rangle + \dot{a}_l \langle q_k \,|\, \frac{\partial}{\partial a_l} q_l \rangle \\ + \dot{\phi}_l \langle q_k \,|\, \frac{\partial}{\partial \phi_l} q_l \rangle + \dot{\chi}_l \langle q_k \,|\, \frac{\partial}{\partial \chi_l} q_l \rangle \end{aligned} \tag{A.18}$$

one needs the following partial derivatives

$$= (1 - \varrho^{(1)}) \sum_{k=1}^{A} \; | \frac{\partial}{\partial q_\mu} q_m \rangle \; \mathcal{O}_{mk} \; \langle \, q_k \, | \; + \; h.a. \; . \tag{A.6}$$

Since the greek subscript $\mu = \{m, i\}$ contains both, the number m of the wave packet and i which labels the parameter within the packet only the state $| \, q_m \, \rangle$ contributes to the the differentiation with respect to q_μ:

$$\frac{\partial}{\partial q_\mu} | \, q_n \, \rangle = \delta_{nm} \; | \frac{\partial}{\partial q_\mu} q_m \rangle \; . \tag{A.7}$$

Furthermore we used the relation

$$\sum_{n=1}^{A} \mathcal{O}_{kn} \; \langle \, q_n \, | \, q_l \, \rangle = \delta_{kl} \tag{A.8}$$

between the overlap matrix $\langle \, q_k \, | \, q_l \, \rangle$ and its inverse $\mathcal{O}_{kl}$ to calculate the derivative of the inverse overlap matrix as

$$\begin{aligned} \frac{\partial}{\partial q_\mu} \mathcal{O}_{kl} &= - \sum_{n,n'=1}^{A} \mathcal{O}_{kn} \; \frac{\partial}{\partial q_\mu} \Big(\langle \, q_n \, | \, q_{n'} \, \rangle \Big) \; \mathcal{O}_{n'l} \\ &= - \sum_{n=1}^{A} \mathcal{O}_{km} \; \langle \; \frac{\partial}{\partial q_\mu} q_m \, | \, q_n \, \rangle \; \mathcal{O}_{nl} - \sum_{n=1}^{A} \mathcal{O}_{kn} \; \langle \, q_n \, | \; \frac{\partial}{\partial q_\mu} q_m \, \rangle \; \mathcal{O}_{ml} \; . \end{aligned} \tag{A.9}$$

By taking the trace of eq. (A.6) with the desired one-body operator one obtains the derivative as given in eq. (49).

The overlap matrix for the single particle states (A.4) is given by

$$\langle \, q_k \, | \, q_l \, \rangle \; = \; \left(2\pi \frac{a_k^* a_l}{a_k^* + a_l} \right)^{3/2} \exp \left\{ - \frac{(\boldsymbol{b}_k^* - \boldsymbol{b}_l)^2}{2 \, (a_k^* + a_l)} \right\} \; S_{kl} \; T_{kl} \tag{A.10}$$

with the spin overlap

$$\begin{aligned} S_{kl} &= \langle \, \chi_k, \phi_k \, | \, \chi_l, \phi_l \, \rangle \\ &= \cos \frac{\chi_k}{2} \cos \frac{\chi_l}{2} \; + \; \sin \frac{\chi_k}{2} \sin \frac{\chi_l}{2} \; e^{-i(\phi_k - \phi_l)} \end{aligned} \tag{A.11}$$

and the isospin overlap

$$T_{kl} = \langle \, m_t(k) \, | \, m_t(l) \, \rangle$$

$$\langle \frac{\partial}{\partial \phi_k} q_k \,|\, \underset{\sim}{t} \,|\, q_l \rangle = -i \sin\frac{\chi_k}{2} \sin\frac{\chi_l}{2} e^{-i(\phi_k-\phi_l)} \frac{\langle q_k \,|\, \underset{\sim}{t} \,|\, q_l \rangle}{\langle \chi_k, \phi_k \,|\, \chi_l, \phi_l \rangle} , \tag{A.27}$$

$$\langle \frac{\partial}{\partial \chi_k} q_k \,|\, \underset{\sim}{t} \,|\, q_l \rangle = \tfrac{1}{2} \Big(-\sin\frac{\chi_k}{2}\cos\frac{\chi_l}{2} + \cos\frac{\chi_k}{2}\sin\frac{\chi_l}{2} e^{-i(\phi_k-\phi_l)} \Big) \frac{\langle q_k \,|\, \underset{\sim}{t} \,|\, q_l \rangle}{\langle \chi_k, \phi_k \,|\, \chi_l, \phi_l \rangle} . \tag{A.28}$$

A.2 A-matrix

The $\mathcal{A}$-matrix defined in eq. (47) is expressed in terms of the inverse overlap matrix and derivatives of the overlaps

$$\mathcal{A}_{\mu\nu} := \frac{\partial^2 \mathcal{L}_0}{\partial \dot{q}_\mu \partial q_\nu} - \frac{\partial^2 \mathcal{L}_0}{\partial \dot{q}_\nu \partial q_\mu} = 2 \,\mathrm{Im}\, \langle \frac{\partial}{\partial q_\mu} Q(t) \,|\, \frac{\partial}{\partial q_\nu} Q(t) \rangle \tag{A.29}$$

$$\begin{aligned} &= 2 \,\mathrm{Im} \left\{ \langle \frac{\partial}{\partial q_\mu} q_m \,|\, \frac{\partial}{\partial q_\nu} q_n \rangle \mathcal{O}_{nm} \right\} \\ &+ \sum_{k=1}^{A} \mathrm{Im} \left\{ \langle \frac{\partial}{\partial q_\mu} q_m \,|\, q_k \rangle \frac{\partial}{\partial q_\nu} \mathcal{O}_{km} \right\} - \sum_{k=1}^{A} \mathrm{Im} \left\{ \langle \frac{\partial}{\partial q_\nu} q_n \,|\, q_k \rangle \frac{\partial}{\partial q_\mu} \mathcal{O}_{kn} \right\} \\ &= 2 \,\mathrm{Im} \Big\{ \mathcal{O}_{nm} \langle \frac{\partial}{\partial q_\mu} q_m \,|\, \frac{\partial}{\partial q_\nu} q_n \rangle \\ &\quad - \mathcal{O}_{nm} \sum_{k,l=1}^{A} \langle \frac{\partial}{\partial q_\mu} q_m \,|\, q_k \rangle \mathcal{O}_{kl} \langle q_l \,|\, \frac{\partial}{\partial q_\nu} q_n \rangle \Big\} . \end{aligned} \tag{A.30}$$

In the following we write down explicitly the 25 matrix elements from which, with help of relation (A.42), one can obtain all the others.

$$\langle \frac{\partial}{\partial b^*_{ki}} q_k \,|\, \frac{\partial}{\partial b_{lj}} q_l \rangle = \left(\frac{\delta_{ij}}{a^*_k + a_l} - \frac{(b^*_{ki} - b_{li})(b^*_{kj} - b_{lj})}{(a^*_k + a_l)^2} \right) \langle q_k \,|\, q_l \rangle \tag{A.31}$$

for the three directions $i, j = 1, 2, 3$.

$$\langle \frac{\partial}{\partial a^*_k} q_k \,|\, \frac{\partial}{\partial a_l} q_l \rangle = \left\{ \frac{1}{2} \left(\frac{3}{a^*_k} - \frac{3}{a^*_k + a_l} + \left(\frac{\boldsymbol{b}^*_k - \boldsymbol{b}_l}{a^*_k + a_l} \right)^2 \right) \cdot \frac{1}{2} \left(\frac{3}{a_l} - \frac{3}{a^*_k + a_l} + \left(\frac{\boldsymbol{b}^*_k - \boldsymbol{b}_l}{a^*_k + a_l} \right)^2 \right) \right.$$

$$\langle q_k \mid \frac{\partial}{\partial \boldsymbol{b}_l} q_l \rangle = \frac{\boldsymbol{b}_k^* - \boldsymbol{b}_l}{a_k^* + a_l} \langle q_k \mid q_l \rangle \,, \tag{A.19}$$

$$\langle q_k \mid \frac{\partial}{\partial a_l} q_l \rangle = \frac{1}{2} \left(\frac{3}{a_l} - \frac{3}{a_k^* + a_l} + \left(\frac{\boldsymbol{b}_k^* - \boldsymbol{b}_l}{a_k^* + a_l} \right)^2 \right) \langle q_k \mid q_l \rangle \,, \tag{A.20}$$

$$\langle q_k \mid \frac{\partial}{\partial \phi_l} q_l \rangle = i \sin \frac{\chi_k}{2} \sin \frac{\chi_l}{2} e^{-i(\phi_k - \phi_l)} \frac{\langle q_k \mid q_l \rangle}{\langle \chi_k, \phi_k \mid \chi_l, \phi_l \rangle} \,, \tag{A.21}$$

$$\langle q_k \mid \frac{\partial}{\partial \chi_l} q_l \rangle = \frac{1}{2} \left(-\cos \frac{\chi_k}{2} \sin \frac{\chi_l}{2} + \sin \frac{\chi_k}{2} \cos \frac{\chi_l}{2} e^{-i(\phi_k - \phi_l)} \right) \frac{\langle q_k \mid q_l \rangle}{\langle \chi_k, \phi_k \mid \chi_l, \phi_l \rangle} \,. \tag{A.22}$$

The matrix elements where the derivative is with respect to parameters in bra can be simply obtained by complex conjugation

$$\langle \frac{\partial}{\partial r_\lambda^*} q_l \mid q_k \rangle = \left(\langle q_k \mid \frac{\partial}{\partial r_\lambda} q_l \rangle \right)^* \,, \tag{A.23}$$

where r_λ is a member of the parameter set $\{\boldsymbol{b}_l, \boldsymbol{b}_l^*, a_l, a_l^*, \phi_l, \chi_l\}$ in which the parameters and their complex conjugate are taken as independent variables.

The one-body matrix element of the kinetic energy has the following form

$$\begin{aligned} \langle q_k \mid \underset{\sim}{t} \mid q_l \rangle &= \langle q_k \mid \frac{\underset{\sim}{\boldsymbol{k}}^2}{2m_N} \mid q_l \rangle \\ &= \frac{1}{2m_N} \left(\frac{3}{2} \frac{2}{a_k^* + a_l} - \left(\frac{\boldsymbol{b}_k^* - \boldsymbol{b}_l}{a_k^* + a_l} \right)^2 \right) \langle q_k \mid q_l \rangle, \end{aligned} \tag{A.24}$$

and its derivatives with respect to parameters in bra are

$$\langle \frac{\partial}{\partial \boldsymbol{b}_k^*} q_k \mid \underset{\sim}{t} \mid q_l \rangle = -\frac{1}{2m} \frac{\boldsymbol{b}_k^* - \boldsymbol{b}_l}{a_k^* + a_l} \left(\frac{5}{a_k^* + a_l} - \left(\frac{\boldsymbol{b}_k^* - \boldsymbol{b}_l}{a_k^* + a_l} \right)^2 \right) \langle q_k \mid q_l \rangle \,, \tag{A.25}$$

$$\begin{aligned} \langle \frac{\partial}{\partial a_k^*} q_k \mid \underset{\sim}{t} \mid q_l \rangle = \Bigg[& \frac{3}{2m} \frac{1}{a_k^* + a_l} \frac{1}{2} \left(\frac{3}{a_k^*} - \frac{5}{a_k^* + a_l} + \left(\frac{\boldsymbol{b}_k^* - \boldsymbol{b}_l}{a_k^* + a_l} \right)^2 \right) \\ & - \frac{1}{2m} \left(\frac{\boldsymbol{b}_k^* - \boldsymbol{b}_l}{a_k^* + a_l} \right)^2 \frac{1}{2} \left(\frac{3}{a_k^*} - \frac{7}{a_k^* + a_l} + \left(\frac{\boldsymbol{b}_k^* - \boldsymbol{b}_l}{a_k^* + a_l} \right)^2 \right) \Bigg] \langle q_k \mid q_l \rangle \,, \end{aligned} \tag{A.26}$$

$$\langle \frac{\partial}{\partial \chi_k} q_k \,|\, \frac{\partial}{\partial a_l} q_l \rangle = \frac{1}{2}\left(\frac{3}{a_l} - \frac{3}{a_k^* + a_l} + \left(\frac{b_k^* - b_l}{a_k^* + a_l}\right)^2\right)$$
$$\frac{1}{2}\left(-\sin\frac{\chi_k}{2}\cos\frac{\chi_l}{2}\right.$$
$$\left.+\cos\frac{\chi_k}{2}\sin\frac{\chi_l}{2}\,e^{-i(\phi_k-\phi_l)}\right)\frac{\langle q_k \,|\, q_l\rangle}{\langle \chi_k, \phi_k \,|\, \chi_l, \phi_l\rangle} \qquad \text{(A.41)}$$

All other mixed second derivatives are obtained by

$$\langle \frac{\partial}{\partial r_\lambda^*} q_l \,|\, \frac{\partial}{\partial r_\kappa} q_k \rangle = \left(\langle \frac{\partial}{\partial r_\kappa^*} q_k \,|\, \frac{\partial}{\partial r_\lambda} q_l \rangle\right)^* , \qquad \text{(A.42)}$$

where r_λ is a member of the parameter set $\{b_l, b_l^*, a_l, a_l^*, \phi_l, \chi_l\}$ in which the parameters and their complex conjugate are taken as independent variables.

A.3 Two-body matrixelements

Analogue to the derivative of the one-body density given in eq. (A.6) one calculates the derivative of the two-body density matrix

$$\underset{\sim}{\rho}^{(2)} = \frac{1}{4}\sum_{k,k',l,l'=1}^{A} |\, q_k, q_l \rangle_a \; \mathcal{O}_{kk'}\,\mathcal{O}_{ll'} \; {}_a\langle\, q_{k'}, q_{l'} \,| \qquad \text{(A.43)}$$

as

$$\frac{\partial \underset{\sim}{\rho}^{(2)}}{\partial q_\mu} = \frac{1}{2}\sum_{k,l,l'=1}^{A} |\, q_k, q_l \rangle_a \; \mathcal{O}_{km}\,\mathcal{O}_{ll'} \; {}_a\langle \frac{\partial}{\partial q_\mu} q_m, q_{l'} \,| \;+\; h.a.$$
$$+\frac{1}{2}\sum_{k,k',l,l'=1}^{A} |\, q_k, q_l \rangle_a \; \mathcal{O}_{kk'}\frac{\partial \mathcal{O}_{ll'}}{\partial q_\mu} \; {}_a\langle\, q_{k'}, q_{l'} \,| \;. \qquad \text{(A.44)}$$

Inserting the derivative of the inverse overlap matrix given in (A.9) yields

$$\frac{\partial \underset{\sim}{\rho}^{(2)}}{\partial q_\mu} = \frac{1}{2}\sum_{k,l,l'=1}^{A} |\, q_k, q_l \rangle_a \; \mathcal{O}_{km}\,\mathcal{O}_{ll'} \; {}_a\langle \frac{\partial}{\partial q_\mu} q_m, q_{l'} \,| \;+\; h.a.$$
$$-\frac{1}{2}\sum_{k,k',l,l',n=1}^{A} |\, q_k, q_l \rangle_a \; \mathcal{O}_{kk'}\,\mathcal{O}_{ln}\langle\, q_n \,|\, \frac{\partial}{\partial q_\mu} q_m \rangle \mathcal{O}_{ml'} \; {}_a\langle\, q_{k'}, q_{l'} \,| \;-\; h.a. \qquad \text{(A.45)}$$

which explains eq. (50).

$$+\frac{1}{a_k^*+a_l}\left(\frac{1}{2}\frac{3}{a_k^*+a_l}-\left(\frac{\boldsymbol{b}_k^*-\boldsymbol{b}_l}{a_k^*+a_l}\right)^2\right)\Bigg\}\langle q_k\,|\,q_l\rangle \tag{A.32}$$

$$\langle\frac{\partial}{\partial a_k^*}q_k\,|\,\frac{\partial}{\partial \boldsymbol{b}_l}q_l\rangle=\frac{\boldsymbol{b}_k^*-\boldsymbol{b}_l}{a_k^*+a_l}\frac{1}{2}\left(\frac{3}{a_k^*}-\frac{5}{a_k^*+a_l}+\left(\frac{\boldsymbol{b}_k^*-\boldsymbol{b}_l}{a_k^*+a_l}\right)^2\right)\langle q_k\,|\,q_l\rangle \tag{A.33}$$

$$\langle\frac{\partial}{\partial\phi_k}q_k\,|\,\frac{\partial}{\partial\phi_l}q_l\rangle=\sin\frac{\chi_k}{2}\sin\frac{\chi_l}{2}e^{-i(\phi_k-\phi_l)}\frac{\langle q_k\,|\,q_l\rangle}{\langle\chi_k,\phi_k\,|\,\chi_l,\phi_l\rangle} \tag{A.34}$$

$$\langle\frac{\partial}{\partial\chi_k}q_k\,|\,\frac{\partial}{\partial\chi_l}q_l\rangle=\frac{1}{4}\left(-\sin\frac{\chi_k}{2}\sin\frac{\chi_l}{2}+\cos\frac{\chi_k}{2}\cos\frac{\chi_l}{2}e^{-i(\phi_k-\phi_l)}\right)\frac{\langle q_k\,|\,q_l\rangle}{\langle\chi_k,\phi_k\,|\,\chi_l,\phi_l\rangle} \tag{A.35}$$

$$\langle\frac{\partial}{\partial\chi_k}q_k\,|\,\frac{\partial}{\partial\phi_l}q_l\rangle=\frac{i}{2}\cos\frac{\chi_k}{2}\sin\frac{\chi_l}{2}e^{-i(\phi_k-\phi_l)}\frac{\langle q_k\,|\,q_l\rangle}{\langle\chi_k,\phi_k\,|\,\chi_l,\phi_l\rangle} \tag{A.36}$$

$$\langle\frac{\partial}{\partial\phi_k}q_k\,|\,\frac{\partial}{\partial\chi_l}q_l\rangle=-\frac{i}{2}\sin\frac{\chi_k}{2}\cos\frac{\chi_l}{2}e^{-i(\phi_k-\phi_l)}\frac{\langle q_k\,|\,q_l\rangle}{\langle\chi_k,\phi_k\,|\,\chi_l,\phi_l\rangle} \tag{A.37}$$

$$\langle\frac{\partial}{\partial\phi_k}q_k\,|\,\frac{\partial}{\partial\boldsymbol{b}_l}q_l\rangle=-i\frac{\boldsymbol{b}_k^*-\boldsymbol{b}_l}{a_k^*+a_l}\sin\frac{\chi_k}{2}\sin\frac{\chi_l}{2}e^{-i(\phi_k-\phi_l)}\frac{\langle q_k\,|\,q_l\rangle}{\langle\chi_k,\phi_k\,|\,\chi_l,\phi_l\rangle} \tag{A.38}$$

$$\langle\frac{\partial}{\partial\chi_k}q_k\,|\,\frac{\partial}{\partial\boldsymbol{b}_l}q_l\rangle=\frac{\boldsymbol{b}_k^*-\boldsymbol{b}_l}{a_k^*+a_l}\frac{1}{2}\left(-\sin\frac{\chi_k}{2}\cos\frac{\chi_l}{2}+\cos\frac{\chi_k}{2}\sin\frac{\chi_l}{2}e^{-i(\phi_k-\phi_l)}\right)\frac{\langle q_k\,|\,q_l\rangle}{\langle\chi_k,\phi_k\,|\,\chi_l,\phi_l\rangle} \tag{A.39}$$

$$\langle\frac{\partial}{\partial\phi_k}q_k\,|\,\frac{\partial}{\partial a_l}q_l\rangle=\frac{1}{2}\left(\frac{3}{a_l}-\frac{3}{a_k^*+a_l}+\left(\frac{\boldsymbol{b}_k^*-\boldsymbol{b}_l}{a_k^*+a_l}\right)^2\right)\left(-i\sin\frac{\chi_k}{2}\sin\frac{\chi_l}{2}e^{-i(\phi_k-\phi_l)}\right)\frac{\langle q_k\,|\,q_l\rangle}{\langle\chi_k,\phi_k\,|\,\chi_l,\phi_l\rangle} \tag{A.40}$$

In the following we present the radial integral and its derivatives:

$$R_{klmn} = (2\pi)^3 \left(\frac{r_1^2 z_{klmn}}{n_{klmn}}\right)^{3/2} \exp\{-\epsilon_{klmn}\} \times \exp\left\{\frac{z_{klmn}}{n_{klmn}}(\boldsymbol{\beta}_{km}+\boldsymbol{\beta}_{ln})^2\right\} \times \exp\left\{\tfrac{1}{2}\frac{r_1^2}{n_{klmn}}(h_{klmn}\boldsymbol{\beta}_{km}^2 + h_{lknm}\boldsymbol{\beta}_{ln}^2)\right\} \quad \text{(A.46)}$$

where we have used the abbreviations

$$\begin{aligned}
\boldsymbol{\beta}_{km} &:= \frac{\boldsymbol{b}_k^*}{a_k^*} + \frac{\boldsymbol{b}_m}{a_m}\,, \\
\epsilon_{klmn} &:= \frac{\boldsymbol{b}_k^{*2}}{2\,a_k^*} + \frac{\boldsymbol{b}_l^{*2}}{2\,a_l^*} + \frac{\boldsymbol{b}_m^2}{2\,a_m} + \frac{\boldsymbol{b}_n^2}{2\,a_n}\,, \\
z_{klmn} &:= a_k^*\, a_l^*\, a_m\, a_n\,, \\
h_{klmn} &:= a_k^*\, a_m\,(a_l^* + a_n)\,, \\
n_{klmn} &:= r_1^2\,(a_k^* + a_m)(a_l^* + a_n) + 2\,a_k^*\, a_m\,(a_l^* + a_n) + 2\,a_l^*\, a_n\,(a_k^* + a_m)\,.
\end{aligned} \quad \text{(A.47)}$$

As already mentioned one needs only the derivatives with respect to the first index k, because all others can be obtained by utilizing the symmetry properties.

$$\frac{\partial}{\partial \boldsymbol{b}_k^*} R_{klmn} = \frac{1}{a_k^*}\left\{-\boldsymbol{b}_k^* + (\boldsymbol{\beta}_{km}+\boldsymbol{\beta}_{ln})\,2\,\frac{z_{klmn}}{n_{klmn}} + r_1^2\,\frac{h_{klmn}}{n_{klmn}}\,\boldsymbol{\beta}_{km}\right\} R_{klmn}, \quad \text{(A.48)}$$

$$\begin{aligned}
\frac{\partial}{\partial a_k^*} R_{klmn} = \Bigg\{ & \frac{3}{2}\left[\frac{1}{z_{klmn}}\left(\frac{\partial z_{klmn}}{\partial a_k^*}\right) - \frac{1}{n_{klmn}}\left(\frac{\partial n_{klmn}}{\partial a_k^*}\right)\right] \\
& - 2\frac{z_{klmn}}{n_{klmn}}(\boldsymbol{\beta}_{km}+\boldsymbol{\beta}_{ln})\cdot\frac{\boldsymbol{b}_k^*}{a_k^{*2}} + \tfrac{1}{2}\left(\frac{\boldsymbol{b}_k^*}{a_k^*}\right)^2 \\
& + \left[\frac{1}{n_{klmn}}\left(\frac{\partial z_{klmn}}{\partial a_k^*}\right) - \frac{z_{klmn}}{n_{klmn}^2}\left(\frac{\partial n_{klmn}}{\partial a_k^*}\right)\right](\boldsymbol{\beta}_{km}+\boldsymbol{\beta}_{ln})^2 \\
& + \tfrac{1}{2}\frac{r_1^2}{n_{klmn}}\left[\frac{\partial h_{klmn}}{\partial a_k^*}\boldsymbol{\beta}_{km}^2 + \frac{\partial h_{lknm}}{\partial a_k^*}\boldsymbol{\beta}_{ln}^2 - h_{klmn}\,2\,\boldsymbol{\beta}_{km}\cdot\frac{\boldsymbol{b}_k^*}{a_k^{*2}}\right] \\
& - \tfrac{1}{2}\left(\frac{r_1}{n_{klmn}}\right)^2\frac{\partial n_{klmn}}{\partial a_k^*}\left(h_{klmn}\boldsymbol{\beta}_{km}^2 + h_{lknm}\boldsymbol{\beta}_{ln}^2\right)\Bigg\} R_{klmn}\,. \quad \text{(A.49)}
\end{aligned}$$

The partial derivatives of the above mentioned abbreviations are:

$$\frac{\partial h_{lknm}}{\partial a_k^*} = a_l^* \, a_n \ ,$$
$$\frac{\partial h_{klmn}}{\partial a_k^*} = a_m \, (\, a_l^* + a_n \,) \ , \qquad \text{(A.50)}$$
$$\frac{\partial z_{klmn}}{\partial a_k^*} = a_l^* \, a_m \, a_n \ ,$$
$$\frac{\partial n_{klmn}}{\partial a_k^*} = r_1^2 \, (\, a_l^* + a_n \,) + 2 \, a_l^* \, a_n + 2 \, a_m \, (\, a_l^* + a_n \,) \ .$$

References

[1] J.P. Bondorf, H.T. Feldmeier, S. Garpman, E.C. Halbert, Phys. Lett. **65B** (1976) 217

[2] L. Wilets, Y. Yariv, R. Chestnut, Nucl. Phys. **A301** (1978) 359
L. Wilets, E.M. Henley, M. Kraft, A.D. MacKellar,
Nucl. Phys. **A282** (1977) 341
L. Wilets, A.D. MacKellar, G.A. Rinker Jr., Proc.IV Int. Workshop on Gross Properties of Nuclei and Nuclear Excitations, Hirschegg Austria (1976) p. 111
ISSN 0720-8715

[3] A.R. Bodmer, C.N. Panos, Phys. Rev. **C15** (1977) 1342

[4] J.J. Molitoris, J.B. Hoffer, H. Kruse, H. Stöcker,
Phys. Rev. Lett. **53** (1984) 899

[5] J. Aichelin, H. Stöcker, Phys. Lett. **B176** (1986) 14

[6] J. Aichelin, Phys. Rep. **202** (1991) 233

[7] A. Ono, H. Horiuchi, T. Maruyama, A. Ohnishi,
Phys. Rev. Lett. **68** (1992) 2898

[8] A. Ono, H. Horiuchi, T. Maruyama, A. Ohnishi,
Prog. Theor. Phys. **87** (1992) 1185

[9] A. Ono, H. Horiuchi, T. Maruyama, Phys. Rev. **C48** (1994) 2946

[10] H. Feldmeier, Nucl. Phys. **A515** (1990) 147

[11] D.H. Boal, J.N. Glosli, Phys. Rev. **C38** (1988) 1870
D.H. Boal, J.N. Glosli, C. Wicentowich, Phys. Rev. **C40** (1989) 601

[12] C. Dorso, S. Duarte, J. Randrup, Phys. Lett. **B188** (1987) 287

[13] C. Dorso, J. Randrup, Phys. Lett. **B215** (1987) 611

[14] C. Hartnack, Li Zhuxia, L. Neise, G. Peilert, A. Rosenhauer, H. Sorge, J. Aichelin, H. Stöcker, W. Greiner, Nucl. Phys. **A495** (1989) 303c

[15] V.I. Arnol'd, Mathematical Methods of Classical Mechanics, Springer-Verlag Berlin (1989)

[16] C. Coriano, R. Parwani, H. Yamagishi, Nucl. Phys. **A522** (1991) 591

[17] P. Kramer, M. Saraceno, Lecture Notes in Physics **140**, Springer, Berlin (1981)

[18] J. Broeckhove, L. Lathouwers, P. van Leuven,
J. Phys. A: Math. Gen. **22** (1989) 4395

[19] A.B. Volkov, Nucl.Phys. **74** (1965) 33

[20] D.M. Brink, E. Boeker, Nucl. Phys. **A91** (1967) 1

[21] C.M. Lederer, V.S. Shirley, Table of Isotopes 7^{th} ed. (1978), John Wiley & Sons, INC. New York

[22] H. de Vries, C.W. de Jager and C. de Vries, Atomic Data and Nuclear Data Tables **36** (1987) 495

[23] H. Feldmeier, K. Bieler, Proc. 1. Europ. Biennial Workshop on Nucl. Phys., Megève, France, World Scientific (1991) p. 125 and preprint GSI-91-29
K. Bieler, diploma thesis, TH Darmstatdt (1991), unpublished

[24] H. Feldmeier, J. Schnack, Proc. Int. Workshop on Dyn. Features of Nuclei, Sitges, Spain (1993) World Scientific, and preprint GSI-93-78
J. Schnack, diploma thesis, GSI report GSI-93-21 (1993)

[25] H. Feldmeier, J. Schnack, in "Multifragmentation", Proc. Int. Workshop XXII, Hirschegg, Austria (1994), eds. H. Feldmeier, W. Nörenberg, p. 207

[26] J. Konopka, G. Peilert, H. Stöcker, W. Greiner, Proc. of the XXIX Int. Winter Meeting, Bormio, Italy (1991)

[27] A. Bohr, B.R. Mottelson, Nuclear Structure I and II, W.A. Benjamin, Inc. (1969, 1975) New York, Amsterdam

[28] G.F. Bertsch, H. Kruse, S. Das Gupta, Phys. Rev. **C29** (1984) 673

[29] G.F. Bertsch, S. Das Gupta, Phys. Rep. **160** (1988) 189

[30] H. Kruse, B.V. Jacak, H. Stöcker, Phys. Rev. Lett. **54** (1985) 289

[31] W. Cassing, V. Metag, U. Mosel, K. Niita, Phys. Rep. **188** (1990) 363

[32] C. Grégoire, B. Remaud, F. Sebille, L. Vinet, Y. Raffray,
Nucl. Phys. **A465** (1987) 317

[33] W. Reisdorf, to be published in Journal of Physics G, Sept. (1994)

[34] R. Vandenbosch, Ann. Rev. Nuc. Part. Sci. **42** (1992) 447

[35] R. Jastrow, Phys. Rev. **98** (1955) 1479